Cranfield

College of Aeronautics Report No.9113
August 1991

Experimental Studies of Vortex Flaps and Vortex Plates

Part 1 0.53m 60 deg Delta Wing

K.Rinoie and J.L.Stollery

Department of Aerodynamics
College of Aeronautics
Cranfield Institute of Technology
Cranfield, Bedford MK43 0AL. England

Cranfield

College of Aeronautics Report No.9113
August 1991

Experimental Studies of Vortex Flaps and Vortex Plates

Part 1 0.53m 60 deg Delta Wing

K.Rinoie and J.L.Stollery

Department of Aerodynamics
College of Aeronautics
Cranfield Institute of Technology
Cranfield, Bedford MK43 0AL. England

ISBN 1 871564 33 6

£8.00

College of Aeronautics

Report No. 9113

Experimental Studies of Vortex Flaps and Vortex Plates

Part.1 0.53m Span 60deg Delta Wing

K. Rinoie* and J.L. Stollery

Department of Aerodynamics

College of Aeronautics

Cranfield Institute of Technology

Cranfield, Bedford, MK43 0AL

August 1991

* Permanent Address:
National Aerospace Laboratory, 7-44-1 Jindaiji-higashi-machi, Chofu, Tokyo, 182, Japan

Abstract

Low-speed wind tunnel tests have been made to investigate the flow around a leading-edge vortex flap at the maximum L/D condition. Tests were also made to measure the performance of the inverted vortex flap and the vortex plate. The force measurements and flow visualization tests were conducted on a 60deg delta wing model.

Results indicate that the lift to drag ratio is a maximum for any given flap deflection angle when the flow comes smoothly onto the deflected vortex flap without forming a large leading-edge separation vortex on the flap surface. The benefit of the vortex plate is seen in the drag results which are smaller than those for the datum wing. This benefit is due to some leading-edge suction acting on the forward facing region between the delta wing and the vortex plate.

Nomenclature

AR	Aspect ratio
Cr	Wing centre-line chord
C_D	Drag coefficient
C_{DO}	C_D at zero lift
C_L	Lift coefficient
g	Vortex plate leading-edge position measured from leading-edge of the wing in the chordwise direction
H.L.	Hinge line
K	Induced drag coefficient
L/D	Lift/Drag ratio
R	Reattachment line
Re_{Cr}	Reynolds number (based on wing centre-line chord)
S	Secondary separation line
U_∞	Free stream velocity
α	Wing incidence
δ_f	Vortex flap deflection angle measured normal to the hinge line

1. Introduction

A sharp-edged delta wing is often used for supersonic cruise aircraft because of its good supersonic performance. At subsonic speeds and particularly at take-off and landing, it is necessary for the delta wing aircraft to fly at a high incidence, in order to generate sufficient lift. At high incidence the flow separates from the leading-edges of the wing, wraps up and forms a pair of vortices over the upper surface. Each vortex is called a leading-edge separation vortex. The leading-edge separation vortex produces a large suction force over the wing which increases the lift component. However, there is also a high drag component associated with this suction force. Therefore the lift/drag ratio of the delta wing at low speeds is relatively poor.

The leading-edge vortex flap (LEVF) is one of the devices which can improve the aerodynamic efficiency of delta wings at low speeds (ref.1). The LEVF is a full span deflectable flap attached to the leading-edge of the delta wing. With the flap deflected downward, a leading-edge separation vortex can be formed over the forward facing flap surface, as is shown in fig.1a. The vortex suction force acting normal to the flap surface generates a thrust component. Hence it reduces the drag of the wing and improves the lift/drag ratio at a given lift coefficient, which is essential to the improvement of the take off and climb performance of delta wing aircraft.

Many tests have been done which confirm the benefit of the LEVF (refs.1, 2 and 3). Ref.4 presents an overview of recent LEVF research. Tests have been made at the College of Aeronautics (refs.5, 6 and 7) using two 60deg delta wing models with tapered vortex flaps, in order to study the optimum flap size and the optimum flap deflection angle. All these experiments (refs.1-7) showed that the LEVF can give appreciable improvements in the lift/drag ratio over a wide range of incidence

and confirmed the potential benefit of the vortex flap. It was suggested in ref.2 that the best L/D performance is obtained when the flow separates at the leading-edge of the vortex flap and reattaches near the wing-flap hinge line. Thus the spiral leading-edge vortex is located entirely over the flap as is shown in fig.1a. However, it was suggested in ref.7 that the optimum lift to drag ratio is achieved with the flow coming smoothly onto the deflected LEVF, i.e. there is no vortex above or below the flap surface.

In this paper, experiments were conducted to gain more understanding of the complex flow around the LEVF. The delta wing model tested is the same as used in ref.5. Three different flap deflection angles were used in order to study the flow pattern differences around the LEVF.

When the LEVF is deflected upward instead of downward, it is expected that the leading-edge separation vortex would be formed at a lower incidence than for the normal wing (fig.1b). This vortex can increase not only the drag but also the lift at a low incidence. This large lift and drag component at low incidence might be helpful for the landing situation (ref.8). Hence in this report the inverted LEVF configuration was also tested.

Rao & Johnson (ref.9) showed that a vortex plate, a type of leading-edge split flap, can also give substantial amounts of leading-edge thrust. The vortex plate is a thin plate attached to the lower surface of the leading-edge of the delta wing as is shown in fig.1c. At positive incidence separation occurs at the leading-edge of the vortex plate and at a particular incidence a spanwise vortex can form just in front of the leading-edge of the wing with the reattachment line along the leading-edge. This vortex induces a suction in the cavity between the delta wing and the vortex plate and so reduces the drag. In this paper, tests were made to improve the understanding of how the vortex plate works.

In summary, the purpose of this research is

1) to gain more understanding of the flow around the LEVF, in order to determine the condition for the optimum L/D,

2) to discover the characteristics of the inverted vortex flap,

3) to investigate the benefits of the vortex plate.

2. Experimental Details

Fig.2 shows the model details. This model is the same one that was tested in ref.5. The model is a 60deg flat delta wing having no camber. The centre-line chord length Cr is 457mm and the thickness is 12.7mm. The model is made of plywood. The upper and lower surfaces of all edges are cut away so that the edges are sharp and have an apex angle of 34.4deg, where this angle is measured in a plane normal to the edge concerned. The model has the LEVF hinge lines running from the wing apex to 75% of the trailing-edge semispan station. In ref.5, two different model types which have 50% and 75% hinge line were tested. Results showed the 75% model has a better performance than that of the 50% model. Therefore, only the 75% hinge line model was used in this experiment. In ref.5, several configurations which have different flap deflection angle δ_f were tested. The angle δ_f is defined as the angle measured in the plane normal to the hinge line. It was shown in ref.5 that the maximum L/D was achieved with δ_f=10deg. In order to study the flow differences between the optimum configuration and those with larger flap deflection angles, the flap configurations δ_f=10deg, 15deg and 30deg were tested. The inverted LEVF cases were measured at δ_f=-10deg and -30deg.

The vortex plate (fig.3) is made of 1mm thickness aluminium plate and has a sharp leading-edge. The plan shape is the same as that of the leading-edge region of the delta wing model and the width of the plate is 48mm. The plate was attached to the lower surface of the datum model (no LEVF deflection). The plate can be moved forward as shown in fig.3. The position of the plate is defined by the chordwise distance g between the leading-edge of the wing and that of the vortex plate. In these tests the plate was set at g/Cr=0., 0.01 and 0.02. The position g/Cr=0. means that the leading-edge of the vortex plate coincides with the leading-edge of the wing in plan view.

The experiments were done in the 1m x 0.69m low-speed open-jet wind tunnel. Lift and drag were measured using a T.E.M. three-component wind tunnel balance and the tunnel micro-computer data acquisition system. Measurements were made at tunnel speeds of U_∞ =20m/s and 30m/s. The Reynolds numbers based on the wing centreline chord were 6.1×10^5 and 9.1×10^5, respectively. The incidence of the model α was increased from -14deg until the stall occurred (about 34deg). The model was mounted on twin shielded struts with a tail-sting for incidence control. A picture of the model, the tunnel balance and the wind tunnel is shown in fig.4.

The T.E.M. balance was calibrated before the experiments. The strut tare effect was taken into account and tunnel boundary corrections were applied to the measured data. The solid and wake blockage effects were corrected using the approximate method described in ref.10. The lift effect was corrected according to ref.11. The effect of static pressure gradient was neglected because the tunnel is of the open-jet type. Interference between the struts and the model was not accounted for.

The aerodynamic coefficients were calculated for every flap deflection angle, based on the same total projected wing area with no LEVF deflection. In many studies, the vortex flap is attached to the leading-edge of the delta wing, which causes an increase in model area. In our tests a hinged flap was fitted and the datum delta wing area was used in calculating all aerodynamic coefficients. For the vortex plate measurements, the datum wing area was used as a basis, even though the total area of the model is greater than that of the datum wing for g/Cr=0.01 and 0.02.

Flow visualization tests using the surface oil flow, smoke filament and flying tuft techniques were very helpful in describing the flow around the LEVF.

3. Results and Discussion

The tabulated data including incidence, lift, and drag coefficients with and without tunnel wall corrections are presented in table 1.

3.1 Vortex Flap

The C_L vs. α curves are shown in fig.5 for various LEVF deflection angles δ_f at Reynolds numbers of 6.1×10^5 and 9.1×10^5. Because of load restrictions on the tunnel balance, incidences greater than about 15deg at $Re_{Cr}=9.1 \times 10^5$ could not be used. Figure 5 shows that the C_L decreases as the LEVF is deflected downwards at both Reynolds numbers. Similarly the C_L increases as the LEVF is deflected upwards. Some 'bumps' are observed near the region of α=0deg (δ_f=0deg), α=5deg (δ_f=10deg) and α=10deg (δ_f=-30deg) for $Re_{Cr}=6.1 \times 10^5$. These 'bumps' diminish or reduce at the same incidence position for $Re_{Cr}=9.1 \times 10^5$. The separated shear layer on the wing at the lower Reynolds number is thicker than that at the higher Reynolds number and so may have a greater effect on the C_L vs. α curves at the lower value of Re_{Cr}.

The C_L is not zero at α=0deg for the datum wing although the model is symmetrical. The reason for this is probably the two tunnel struts under the model which affect the flow pattern. Similarly the C_L-α curves for α positive and δ_f= -10deg and -30deg should be similar to the curves for α negative and δ_f=10deg and 30deg. Any differences reflect the effects of strut interference.

Fig.6 shows the C_D vs. α curves. Both Reynolds number cases show similar results. As δ_f increases the C_D decreases for most of the positive incidence region. Similarly C_D increases as the flap is deflected upward. Fig.6 shows that the incidence when the C_D is a minimum, increases as the flap is deflected downwards.

The reason is explained as follows. As is seen in fig.5, the incidence at which the C_L becomes zero increases, as the flap deflection angle increases. Usually the minimum drag is attained when the C_L is close to zero. Therefore, the incidence for the minimum C_D increases as δ_f increases.

Fig.7 shows the lift to drag ratio (L/D) versus C_L. Both Reynolds number cases show similar results. Again any lack of symmetry (when expected) is probably due to strut interference. For flap deflection angles of 10deg and 15deg, the maximum L/D value is greater than that of the datum wing. The L/D attains an absolute maximum at $C_L=0.25$ with $\delta_f=10$deg. This result agrees with that in ref.5. The L/D ratios with $\delta_f=10$deg and 15deg are larger than those of the datum wing for all C_L's>0.2.

Figs.8 and 9 show the surface flow patterns sketched from oil flow pictures for both upper and lower surfaces at $Re_{Cr}=9.1\times10^5$. The patterns define the vortex positions on the wing and flap surfaces. In these figures, H.L. denotes the hinge line, R the reattachment line and S the secondary separation line of the vortex. The hatched region denotes a small separation bubble. In this bubble the oil moved very little. The flow separation region was confirmed by the smoke filament and flying tuft tests. In fig.8 ($\delta_f=10$deg), at an incidence of -3.6deg, a leading-edge separation vortex, which is clearly recognized by the reverse flow region between reattachment line and secondary separation line, is formed on the lower surface. There is no vortex on the upper surface. The same flow should be formed at $\alpha=+3.6$deg with the vortex flap deflected upwards 10 degrees. From $\alpha=0.1$deg to 5.6deg there are only small separation bubbles (hatched region) and the flow comes smoothly onto the flap with no large vortex being formed on either surfaces. At $\alpha=7.5$deg the leading-edge separation vortex is observed in the tip region of the upper surface. At $\alpha=9.3$deg a large separation vortex is formed over the whole of the vortex flap upper surface.

In fig.9 (δ_f=30deg), at the incidences -3.6deg and 2.0deg, the leading-edge separation vortex is formed on lower surface of the model. At α=5.7deg, on the upper surface, it flows smoothly over the flap surface but a separation occurs near the flap hinge line and the separation vortex is formed over the wing. The same tendency is seen at α=9.5deg. At α=13.2deg and 15.1deg, where the visualization was done only on the upper surface, the reverse flow region is observed not only on the wing surface but also on part of the vortex flap. Thus at high incidences a large leading-edge vortex covers much of the model top surface.

Figs.10 and 11 show some C_D vs. C_L curves together with the corresponding flow pattern sketches in the transverse plane. These were deduced from flow visualization using the smoke filament and surface oil flow patterns (figs. 8 and 9). In fig.10, at δ_f=10deg from α=0.1deg to 5.6deg there is only a small separation bubble on the upper surface and the flow comes smoothly onto the flap with no large vortex being formed. For the datum wing, it was observed in flow visualization tests that the leading-edge separation vortex begins to form at α=5.5deg. For δ_f=10deg, the L/D attains the maximum value when the incidence is 5.6deg with no large vortex being formed. The non-existence of the large separation vortex at this incidence means that the wing has a smaller drag than that for the datum wing on which the leading-edge separation vortex is formed at almost the same incidence. Fig.10 shows that C_D at α=5.6deg for δ_f=10deg is almost the same as that for the datum wing at α=3.6deg when there is no leading-edge separation vortex, and the datum wing achieves its maximum L/D ratio. However, C_L at α=5.6deg for δ_f=10deg is larger than that of the datum wing at α=3.6deg, because of the higher incidence. Hence this larger C_L at a similar value of C_D makes L/D for δ_f=10deg much higher than that of the datum wing.

At higher incidence eg α=9.3deg, it is seen that the leading-edge separation vortex is formed over the wing and flap surface. The suction effect of the vortex,

formed on the forward facing flap surface, causes the C_D to be smaller than that of the datum wing, as was explained in ref.1.

With the larger vortex flap deflection of 30deg (fig.11), when C_L is less than 0, the leading-edge separation vortex is formed under the wing causing a large increase in C_D over that of the datum wing. From α=5.7deg to 9.5deg it is observed that the flow comes smoothly onto the deflected leading-edge without forming a large leading-edge separation vortex on the flap surface. However, the flow does separate at the flap hinge line and the vortex is formed inboard of that line. For the datum wing, the same C_L as at α=5.7 to 9.5deg for δ_f=30deg is attained at lower incidence (α is less than 5.5deg), and at these incidences it was observed that there is no leading-edge separation vortex on the datum wing. The existence of the vortex on the inboard wing for δ_f=30deg causes much higher drag than that of the datum wing. The maximum L/D for δ_f=30deg is achieved at an incidence of 9.5deg, but because of the inboard vortex, the value of (L/D)max is lower than that for δ_f=10deg. At α=15.1deg where a large leading-edge separation vortex is formed on the flap as well as on the wing, the suction effect over the flap surface reduces C_D below that of the datum wing. Consequently L/D is larger as shown in fig.7.

3.2 Vortex Plate

Fig.12 shows the C_L vs. α curves for various chordwise vortex plate positions together with the datum wing. It is seen that the results at $Re_{Cr}=6.1x10^5$ and $9.1x10^5$ are almost the same. The effect of the vortex plate at any of the three positions tested is quite small at positive incidence.

When the incidence is between -5deg and -14deg, the C_L is reduced below that of the datum wing. A strong vortex is observed by the flow visualization tests on the lower surface of the vortex plate and the wing. This increased suction substantially reduces the lift (ie increases the lift downwards). This suggests that the better lift component would be gained, when the vortex plate is attached to the upper surface of the datum model.

Fig.13 shows the C_D vs. α curves. Again, there is little difference between the results at $Re_{Cr}=6.1x10^5$ and $9.1x10^5$. However this figure does show that the drag with the vortex plate fitted is smaller than that of the datum wing at positive incidences, which agrees with the results in ref.9. For negative incidences the C_D values with vortex plates fitted are greater than that of the datum wing because of the existence of the strong leading-edge separation vortex on the lower surface of the vortex plate.

Fig.14 illustrates the lift to drag ratio versus C_L for the vortex plate fitted to the wing. Results show that the maximum value of L/D is reduced in comparison with the datum wing for both Reynolds number cases. However, it is seen that the L/D ratio is improved for all C_L values greater than about 0.35, especially for the case of g/Cr=0.02. It is noted that the effect of wing area increase does not affect the L/D value because this is a pure ratio of forces. When compared with the

vortex flap results (fig.7), the L/D for g/Cr=0.02 at C_L's greater than 0.35 is roughly comparable to that of the vortex flap deflected 30deg downward.

Fig.15 sketches the upper surface oil flow patterns for the datum wing, with and without a vortex plate, at incidences from 3.7deg to 22.3deg. The Reynolds number was 6.1×10^5. From this figure it is seen that the onset of the leading-edge separation vortex is between α=3.7 and 5.5deg for the datum wing, at α=5.5deg for g/Cr=0, at α=7.3deg for g/Cr=0.01 and at α=9.2deg for g/Cr=0.02. This means that the onset of the leading-edge separation vortex is delayed by the vortex plate, the delay increasing as g/Cr increases.

Fig.16 gives some indication of the leading-edge suction recoverable through vortex plate deployment. The maximum drag which corresponds to no leading-edge suction is:

$$C_D = C_{D_0} + C_L \cdot \tan\alpha,$$

where C_{D_0} is the zero-lift drag, which depends on the surface skin friction and the form drag. On the other hand, a wing with a well rounded leading-edge and no flow separation could have a drag coefficient described by:

$$C_D = C_{D_0} + KC_L^2 / (\pi AR),$$

where AR is the aspect ratio and $(KC_L^2/(\pi AR))$ is the lift induced drag for attached flow with 100% leading-edge suction. K=1.014 is estimated from ESDU data sheets (ref.12). Using the C_{D_0} measured in the present tests, C_D for the 0% and the 100% leading-edge suction are plotted as C_D vs. α curves for the datum wing (fig.16a) and g/Cr=0.02 (fig.16b). In order to plot the 100% leading-edge suction on C_D vs. α curves in fig.16, it was assumed that $(dC_L/d\alpha)$ is equal to the measured value. For the datum wing, the measured value agrees with 0% leading-edge suction value quite well for 0deg$< \alpha <$20deg region. For g/Cr=0.02 the measured value is less than the 0% leading-edge suction case for 0deg$< \alpha <$30deg region, which suggests that by incorporating the vortex plate some leading-edge

suction is recovered. This reduces the C_D as was seen in fig.13 and improves the L/D ratio as was seen in fig.14. Ref.12 suggested the existence of a separation vortex between the leading-edge of the wing and that of the vortex plate, but the smoke filament visualization tests here did not confirm the existence of a vortex. However, it seems that a separated flow acting on the forward facing region between the vortex plate and the wing produces some leading-edge suction force.

4. Conclusions

Lift and drag measurements were made at Reynolds numbers of 6.1×10^5 and 9.1×10^5 based on the centreline chord. The results showed that there are no major differences between the two sets of tests.

1) The L/D ratio reaches a maximum for any given flap deflection angle when the flow comes smoothly onto the vortex flap without forming a large separation vortex over the flap surface, as was suggested in ref.6. The highest (L/D)max was achieved at a flap deflection angle of 10deg.

2) At high incidences a leading-edge separation vortex is formed on the LEVF surface at every flap deflection angle. Because of the suction effect of this separation vortex, the L/D is higher than that of the datum wing, as was suggested in ref.1.

3) By incorporating the inverted vortex flap, both the lift and the drag can be increased above the datum wing values at the same incidence. However the L/D ratio is reduced.

4) By incorporating the vortex plate, the L/D ratio for all ranges of C_L greater than 0.3 is significantly improved. The vortex plate performance for g/Cr=0.02 is roughly comparable to that of the vortex flap deflected 30deg downward. The measured C_D suggests that some leading-edge suction acts on the wing and so reduces the drag. The occurrence of the leading-edge separation vortex on the wing is delayed when a protruding vortex plate is used.

References

1) Rao, D.M. Leading Edge Vortex-Flap Experiments on a 74deg. Delta Wing, NASA CR-159161, 1979.

2) Rao, D.M. Leading-Edge 'Vortex Flaps' for Enhanced Subsonic Aerodynamics of Slender Wings, ICAS-80-13.5, 1980.

3) Marchman III, J.F. Effectiveness of Leading-Edge Vortex Flaps on 60 and 75 Degree Delta Wings, J.Aircraft, Vol.18, No.4, pp.280-286, 1981.

4) Campbell, J.F. and Osborn, R.F. Leading-Edge Vortex Research: Some Nonplanar Concepts and Current Challenges, NASA CP-2416, pp.31-63, 1986.

5) Ellis, D.G. The Behaviour and Performance of Leading Edge Vortex Flaps, College of Aeronautics Report No.8601, Cranfield, Feb. 1986.

6) Ellis, D.G. and Stollery, J.L. The Behaviour and Performance of Leading-Edge Vortex Flaps, ICAS-88-4.5.2, 1988.

7) Stollery, J.L. and Ellis, D.G. The Behaviour and Performance of Vortex Flaps, College of Aeronautics Report No.NFP8914, Cranfield, Nov. 1989.

8) Marchman III, J.F. Aerodynamics of Inverted Leading-Edge Flaps on Delta Wings, J.Aircraft, Vol.18, No.12, pp.1051-1056, 1981.

9) Rao, D.M. and Johnson Jr., T.D. Investigation of Delta Wing Leading-Edge Devices, J.Aircraft, Vol.18, No.3, pp.161-167, 1981.

10) Rae Jr., W.H. and Pope, A. Low-Speed Wind Tunnel Testing (2nd Ed.), JOHN WILEY & SONS, New York, 1984.

11) Pankhurst, R.C. and Holder. D.W. Wind-Tunnel Technique; an Account of Experimental Methods in Low- and High-Speed Wind Tunnels, PITMAN, London, 1952.

12) ESDU. Subsonic Lift-Dependent Drag Due to the Trailing Vortex Wake for Wings without Camber or Twist, Engineering Sciences Data Unit Item, No.74035, London, 1974.

Table.1 Wind Tunnel Data (Uncorrected & Corrected)

1-1) Datum Wing U_∞=20m/s

Uncorrected			Corrected			
α	CL	CD	α	CL	CD	L/D
-14.0	-.581	.136	-12.857	-.586	.126	-4.652
-12.0	-.492	.099	-11.033	-.496	.092	-5.408
-10.0	-.414	.073	-9.186	-.417	.068	-6.171
-8.0	-.342	.051	-7.328	-.344	.047	-7.292
-6.0	-.271	.035	-5.468	-.273	.032	-8.422
-4.0	-.179	.024	-3.649	-.180	.022	-8.002
-2.0	-.051	.016	-1.901	-.051	.016	-3.092
.0	.036	.016	-.070	.036	.016	2.264
2.0	.137	.019	1.733	.137	.018	7.644
4.0	.203	.024	3.603	.204	.023	8.996
6.0	.269	.037	5.473	.270	.035	7.730
8.0	.340	.057	7.334	.342	.054	6.342
10.0	.417	.083	9.181	.420	.077	5.431
12.0	.488	.115	11.040	.492	.108	4.558
14.0	.558	.153	12.903	.563	.143	3.927
16.0	.616	.193	14.786	.623	.181	3.432
18.0	.691	.243	16.637	.699	.229	3.045
20.0	.758	.300	18.503	.767	.283	2.708
22.0	.827	.364	20.366	.838	.345	2.428
24.0	.886	.431	22.248	.898	.410	2.192
26.0	.943	.503	24.134	.957	.479	1.998
28.0	.995	.582	26.030	1.010	.556	1.817
30.0	1.020	.649	27.979	1.037	.623	1.663
32.0	1.003	.696	30.011	1.020	.673	1.517
34.0	.955	.718	32.104	.972	.699	1.391

1-2) Datum Wing U_∞=30m/s

Uncorrected			Corrected			
α	CL	CD	α	CL	CD	L/D
-14.0	-.588	.136	-12.844	-.593	.126	-4.716
-12.0	-.493	.099	-11.030	-.497	.091	-5.469
-10.0	-.413	.069	-9.189	-.416	.063	-6.557
-8.0	-.315	.044	-7.383	-.317	.041	-7.727
-6.0	-.227	.028	-5.554	-.229	.026	-8.824
-4.0	-.123	.018	-3.758	-.124	.018	-6.941
-2.0	-.048	.015	-1.906	-.048	.015	-3.306
.0	.029	.014	-.057	.029	.014	2.092
2.0	.121	.017	1.763	.122	.017	7.290
4.0	.180	.022	3.647	.181	.021	8.741
6.0	.244	.036	5.522	.245	.034	7.232
8.0	.315	.055	7.382	.317	.051	6.158
10.0	.387	.080	9.239	.390	.075	5.187
12.0	.460	.113	11.096	.463	.107	4.333
14.0	.529	.154	12.958	.534	.145	3.672

2-1) Vortex Flap: δ_f=10deg U_∞=20m/s

Uncorrected			Corrected			
α	CL	CD	α	CL	CD	L/D
-14.0	-.634	.163	-12.753	-.640	.151	-4.239
-12.0	-.578	.134	-10.864	-.582	.124	-4.707
-10.0	-.488	.098	-9.042	-.491	.091	-5.413
-8.0	-.407	.072	-7.201	-.410	.067	-6.145
-6.0	-.314	.049	-5.383	-.316	.046	-6.822
-4.0	-.196	.028	-3.616	-.197	.027	-7.345
-2.0	-.124	.021	-1.757	-.125	.020	-6.168
.0	-.036	.017	.071	-.037	.017	-2.173
2.0	.048	.016	1.907	.048	.016	2.942
4.0	.146	.020	3.714	.147	.019	7.743
6.0	.253	.028	5.505	.254	.026	9.784
8.0	.320	.042	7.373	.322	.039	8.354
10.0	.391	.063	9.232	.394	.058	6.761
12.0	.463	.092	11.089	.467	.086	5.461
14.0	.527	.125	12.963	.532	.116	4.581
16.0	.604	.168	14.811	.610	.157	3.887
18.0	.671	.209	16.676	.679	.196	3.466
20.0	.743	.267	18.535	.751	.251	2.993
22.0	.808	.325	20.404	.818	.307	2.670
24.0	.871	.390	22.279	.882	.369	2.394
26.0	.924	.460	24.172	.937	.437	2.143
28.0	.977	.536	26.066	.992	.511	1.942
30.0	1.010	.608	27.999	1.026	.582	1.764
32.0	1.001	.662	30.015	1.018	.638	1.597
34.0	.990	.710	32.035	1.008	.688	1.464

2-2) Vortex Flap: δ_f=10deg U_∞=30m/s

Uncorrected			Corrected			
α	CL	CD	α	CL	CD	L/D
-14.0	-.629	.161	-12.762	-.635	.149	-4.263
-12.0	-.596	.134	-10.827	-.601	.123	-4.889
-10.0	-.501	.098	-9.017	-.504	.090	-5.625
-8.0	-.396	.069	-7.223	-.398	.064	-6.215
-6.0	-.284	.045	-5.443	-.285	.042	-6.767
-4.0	-.197	.027	-3.615	-.197	.025	-7.750
-2.0	-.114	.019	-1.778	-.114	.019	-6.123
.0	-.030	.015	.059	-.030	.015	-2.010
2.0	.052	.014	1.898	.052	.014	3.623
4.0	.123	.017	3.759	.124	.016	7.579
6.0	.216	.024	5.576	.217	.023	9.597
8.0	.261	.035	7.487	.263	.033	8.068
10.0	.341	.056	9.330	.343	.052	6.565
12.0	.414	.085	11.185	.418	.079	5.258
14.0	.477	.118	13.061	.482	.111	4.330
16.0	.567	.167	14.883	.573	.157	3.638

3-1) Vortex Flap: δ_f=15deg U_∞=20m/s

Uncorrected			Corrected			
α	C_L	C_D	α	C_L	C_D	L/D
-14.0	-.630	.171	-12.760	-.636	.159	-3.999
-12.0	-.586	.141	-10.847	-.591	.130	-4.537
-10.0	-.509	.110	-8.999	-.513	.102	-5.044
-8.0	-.400	.078	-7.215	-.402	.073	-5.520
-6.0	-.287	.052	-5.437	-.289	.050	-5.795
-4.0	-.208	.035	-3.593	-.209	.033	-6.255
-2.0	-.115	.023	-1.776	-.115	.022	-5.137
.0	-.047	.019	.093	-.048	.019	-2.522
2.0	.042	.017	1.919	.042	.017	2.497
4.0	.111	.018	3.783	.111	.018	6.208
6.0	.195	.024	5.618	.196	.023	8.711
8.0	.282	.034	7.446	.284	.031	9.128
10.0	.339	.048	9.335	.341	.044	7.723
12.0	.413	.071	11.187	.417	.066	6.308
14.0	.488	.105	13.040	.492	.098	5.022
16.0	.554	.141	14.908	.560	.132	4.239
18.0	.631	.187	16.755	.638	.175	3.649
20.0	.688	.236	18.642	.696	.223	3.127
22.0	.756	.291	20.507	.766	.275	2.785
24.0	.830	.365	22.360	.841	.346	2.429
26.0	.889	.433	24.240	.902	.411	2.195
28.0	.944	.512	26.131	.958	.489	1.960
30.0	.996	.596	28.027	1.012	.570	1.774
32.0	1.006	.661	30.005	1.023	.636	1.608
34.0	.999	.718	32.016	1.017	.696	1.462
36.0	.949	.743	34.116	.966	.725	1.332

3-2) Vortex Flap: δ_f=15deg U_∞=30m/s

Uncorrected			Corrected			
α	C_L	C_D	α	C_L	C_D	L/D
-14.0	-.623	.169	-12.774	-.629	.158	-3.992
-12.0	-.583	.138	-10.853	-.588	.127	-4.625
-10.0	-.496	.105	-9.025	-.500	.098	-5.125
-8.0	-.387	.074	-7.241	-.389	.069	-5.643
-6.0	-.283	.050	-5.444	-.285	.047	-6.037
-4.0	-.185	.030	-3.638	-.185	.029	-6.388
-2.0	-.105	.019	-1.794	-.106	.019	-5.508
.0	-.042	.016	.082	-.042	.016	-2.568
2.0	.037	.015	1.927	.037	.015	2.472
4.0	.111	.016	3.783	.111	.016	6.902
6.0	.178	.021	5.651	.179	.020	8.879
8.0	.259	.031	7.492	.260	.029	9.118
10.0	.309	.045	9.393	.311	.042	7.442
12.0	.386	.069	11.241	.389	.065	6.029
14.0	.460	.104	13.094	.464	.097	4.779
16.0	.526	.140	14.964	.531	.132	4.033
18.0	.602	.190	16.812	.609	.179	3.396

4-1) Vortex Flap: δ_f=30deg U_∞=20m/s

Uncorrected			Corrected			
α	CL	CD	α	CL	CD	L/D
-14.0	-.517	.168	-12.982	-.522	.160	-3.261
-12.0	-.501	.148	-11.016	-.505	.141	-3.586
-10.0	-.468	.126	-9.081	-.471	.120	-3.941
-8.0	-.395	.099	-7.225	-.397	.095	-4.201
-6.0	-.287	.071	-5.438	-.288	.068	-4.227
-4.0	-.211	.052	-3.586	-.212	.051	-4.155
-2.0	-.140	.040	-1.727	-.140	.039	-3.558
.0	-.072	.029	.142	-.073	.029	-2.500
2.0	.000	.023	2.000	.000	.023	.000
4.0	.068	.024	3.866	.069	.024	2.854
6.0	.140	.028	5.725	.141	.027	5.229
8.0	.215	.034	7.578	.216	.033	6.626
10.0	.278	.043	9.453	.280	.041	6.848
12.0	.340	.054	11.331	.343	.050	6.842
14.0	.411	.069	13.191	.415	.064	6.466
16.0	.478	.092	15.059	.483	.085	5.672
18.0	.542	.128	16.931	.548	.120	4.582
20.0	.621	.173	18.775	.628	.162	3.877
22.0	.697	.225	20.623	.706	.211	3.346
24.0	.765	.283	22.487	.775	.266	2.915
26.0	.843	.354	24.332	.855	.334	2.561
28.0	.909	.425	26.201	.922	.402	2.293
30.0	.958	.500	28.102	.973	.476	2.044
32.0	.970	.565	30.077	.986	.541	1.821
34.0	.986	.631	32.043	1.003	.608	1.651
36.0	.975	.689	34.064	.993	.668	1.486
38.0	.951	.737	36.110	.969	.719	1.347

4-2) Vortex Flap: δ_f=30deg U_∞=30m/s

Uncorrected			Corrected			
α	CL	CD	α	CL	CD	L/D
-14.0	-.501	.166	-13.013	-.506	.159	-3.176
-12.0	-.473	.143	-11.069	-.477	.137	-3.494
-10.0	-.422	.119	-9.171	-.425	.113	-3.753
-8.0	-.367	.095	-7.279	-.369	.090	-4.083
-6.0	-.291	.071	-5.429	-.293	.068	-4.304
-4.0	-.214	.052	-3.581	-.215	.050	-4.280
-2.0	-.139	.038	-1.727	-.140	.037	-3.780
.0	-.070	.026	.136	-.070	.026	-2.675
2.0	.003	.021	1.994	.003	.021	.153
4.0	.069	.022	3.865	.069	.022	3.107
6.0	.137	.026	5.732	.137	.026	5.325
8.0	.209	.033	7.590	.210	.031	6.685
10.0	.275	.043	9.461	.277	.040	6.857
12.0	.336	.055	11.340	.338	.051	6.580
14.0	.393	.070	13.226	.397	.065	6.091
16.0	.452	.091	15.109	.457	.085	5.390
18.0	.520	.128	16.976	.525	.120	4.395

5-1) Vortex Flap: δ_f=-10deg U_∞=20m/s

Uncorrected			Corrected			
α	CL	CD	α	CL	CD	L/D
-14.0	-.546	.111	-12.926	-.551	.101	-5.429
-12.0	-.454	.078	-11.107	-.458	.072	-6.372
-10.0	-.386	.056	-9.242	-.389	.051	-7.648
-8.0	-.312	.039	-7.388	-.314	.036	-8.720
-6.0	-.187	.025	-5.634	-.188	.023	-8.011
-4.0	-.088	.018	-3.828	-.088	.018	-5.041
-2.0	-.007	.016	-1.986	-.007	.016	-.423
.0	.083	.018	-.162	.083	.018	4.556
2.0	.154	.024	1.699	.155	.023	6.611
4.0	.224	.037	3.562	.225	.035	6.411
6.0	.292	.052	5.427	.294	.049	5.939
8.0	.370	.076	7.274	.372	.071	5.210
10.0	.449	.106	9.118	.452	.099	4.550
12.0	.512	.137	10.994	.516	.129	3.988
14.0	.573	.174	12.871	.579	.165	3.517
16.0	.643	.221	14.734	.649	.209	3.109
18.0	.705	.270	16.611	.712	.256	2.786
20.0	.769	.329	18.482	.778	.313	2.490
22.0	.827	.389	20.367	.837	.370	2.266
24.0	.904	.469	22.213	.916	.446	2.052
26.0	.954	.539	24.113	.968	.514	1.881
28.0	.989	.608	26.041	1.004	.582	1.724
30.0	.977	.651	28.063	.993	.628	1.581
32.0	.972	.703	30.072	.988	.682	1.450
34.0	.907	.712	32.200	.923	.695	1.327

5-2) Vortex Flap: δ_f=-10deg U_∞=30m/s

Uncorrected			Corrected			
α	CL	CD	α	CL	CD	L/D
-14.0	-.540	.106	-12.936	-.545	.097	-5.612
-12.0	-.428	.071	-11.158	-.432	.065	-6.653
-10.0	-.358	.048	-9.296	-.361	.044	-8.146
-8.0	-.247	.029	-7.515	-.249	.027	-9.180
-6.0	-.161	.020	-5.683	-.162	.020	-8.263
-4.0	-.091	.016	-3.821	-.092	.016	-5.693
-2.0	-.017	.015	-1.966	-.017	.015	-1.177
.0	.076	.017	-.149	.076	.016	4.677
2.0	.145	.022	1.717	.145	.021	6.790
4.0	.212	.035	3.585	.213	.034	6.341
6.0	.279	.052	5.453	.281	.049	5.702
8.0	.353	.075	7.307	.355	.071	5.014
10.0	.427	.105	9.161	.430	.099	4.332
12.0	.483	.137	11.051	.487	.130	3.739
14.0	.541	.175	12.936	.546	.166	3.281

6-1) Vortex Flap: δ_f=-30deg U_∞=20m/s

Uncorrected			Corrected			
α	CL	CD	α	CL	CD	L/D
-14.0	-.368	.062	-13.275	-.372	.058	-6.433
-12.0	-.302	.048	-11.406	-.304	.045	-6.727
-10.0	-.237	.039	-9.535	-.239	.037	-6.448
-8.0	-.168	.031	-7.670	-.169	.030	-5.685
-6.0	-.093	.026	-5.818	-.093	.026	-3.644
-4.0	-.028	.024	-3.944	-.029	.024	-1.194
-2.0	.042	.029	-2.082	.042	.029	1.440
.0	.105	.036	-.205	.105	.036	2.960
2.0	.187	.049	1.634	.188	.047	3.960
4.0	.261	.066	3.490	.262	.064	4.103
6.0	.346	.088	5.322	.348	.085	4.111
8.0	.437	.121	7.143	.439	.115	3.828
10.0	.519	.156	8.981	.523	.148	3.525
12.0	.584	.195	10.852	.589	.185	3.189
14.0	.627	.229	12.765	.633	.218	2.906
16.0	.691	.279	14.640	.697	.265	2.628
18.0	.754	.332	16.514	.762	.316	2.411
20.0	.815	.393	18.392	.824	.374	2.204
22.0	.865	.450	20.291	.876	.430	2.039
24.0	.908	.515	22.206	.920	.493	1.866
26.0	.945	.580	24.130	.959	.557	1.723
28.0	.966	.635	26.088	.980	.612	1.601
30.0	.931	.667	28.155	.946	.647	1.462
32.0	.897	.690	30.220	.912	.674	1.354
34.0	.829	.687	32.354	.844	.675	1.252

6-2) Vortex Flap: δ_f=-30deg U_∞=30m/s

Uncorrected			Corrected			
α	CL	CD	α	CL	CD	L/D
-14.0	-.376	.061	-13.260	-.379	.057	-6.646
-12.0	-.310	.048	-11.390	-.313	.045	-7.001
-10.0	-.237	.037	-9.534	-.239	.035	-6.778
-8.0	-.168	.029	-7.671	-.169	.028	-5.959
-6.0	-.096	.024	-5.812	-.096	.024	-4.005
-4.0	-.029	.022	-3.944	-.029	.022	-1.295
-2.0	.036	.026	-2.071	.037	.026	1.388
.0	.103	.033	-.201	.103	.033	3.122
2.0	.187	.048	1.634	.188	.047	4.021
4.0	.262	.067	3.487	.263	.065	4.068
6.0	.328	.087	5.357	.330	.084	3.939
8.0	.399	.116	7.217	.402	.112	3.601
10.0	.475	.153	9.068	.478	.146	3.274
12.0	.532	.190	10.954	.536	.182	2.949

7-1) Vortex Plate: g/Cr=0. U_∞=20m/s

Uncorrected			Corrected			
α	CL	CD	α	CL	CD	L/D
-14.0	-.605	.159	-12.809	-.611	.148	-4.122
-12.0	-.570	.133	-10.879	-.575	.122	-4.696
-10.0	-.489	.102	-9.040	-.492	.095	-5.203
-8.0	-.404	.079	-7.208	-.406	.073	-5.531
-6.0	-.306	.055	-5.399	-.308	.052	-5.928
-4.0	-.162	.034	-3.682	-.163	.033	-4.973
-2.0	-.064	.023	-1.874	-.065	.022	-2.874
.0	.011	.018	-.022	.011	.019	.619
2.0	.105	.019	1.794	.105	.019	5.612
4.0	.174	.026	3.660	.174	.025	6.892
6.0	.263	.038	5.485	.264	.036	7.353
8.0	.334	.059	7.344	.336	.055	6.082
10.0	.416	.080	9.183	.419	.075	5.616
12.0	.496	.109	11.024	.500	.102	4.915
14.0	.558	.138	12.901	.563	.129	4.380
16.0	.622	.174	14.774	.628	.162	3.878
18.0	.676	.209	16.667	.683	.195	3.502
20.0	.740	.255	18.540	.749	.239	3.138
22.0	.796	.303	20.429	.806	.285	2.825
24.0	.854	.367	22.311	.866	.347	2.496
26.0	.910	.432	24.199	.923	.410	2.254
28.0	.957	.502	26.105	.971	.478	2.033
30.0	.991	.572	28.035	1.007	.546	1.845
32.0	1.013	.639	29.991	1.030	.613	1.679
34.0	1.017	.703	31.981	1.035	.679	1.525
36.0	.999	.750	34.015	1.018	.729	1.396
38.0	.914	.753	36.183	.931	.738	1.263

7-2) Vortex Plate: g/Cr=0. U_∞=30m/s

Uncorrected			Corrected			
α	CL	CD	α	CL	CD	L/D
-14.0	-.626	.164	-12.769	-.631	.152	-4.148
-12.0	-.583	.136	-10.853	-.588	.126	-4.677
-10.0	-.481	.102	-9.055	-.485	.094	-5.143
-8.0	-.392	.077	-7.230	-.395	.072	-5.484
-6.0	-.265	.050	-5.481	-.266	.048	-5.529
-4.0	-.151	.031	-3.705	-.151	.031	-4.947
-2.0	-.068	.021	-1.867	-.068	.021	-3.230
.0	.012	.017	-.024	.012	.017	.724
2.0	.099	.018	1.806	.099	.018	5.644
4.0	.181	.025	3.646	.181	.024	7.436
6.0	.251	.037	5.507	.253	.035	7.190
8.0	.329	.059	7.355	.331	.056	5.955
10.0	.408	.081	9.199	.411	.075	5.447
12.0	.478	.110	11.059	.482	.103	4.702
14.0	.538	.140	12.941	.543	.132	4.125
16.0	.600	.178	14.817	.606	.168	3.618
18.0	.654	.215	16.710	.661	.203	3.264

8-1) Vortex Plate: g/Cr=0.01 U_∞=20m/s

Uncorrected			Corrected			
α	CL	CD	α	CL	CD	L/D
-14.0	-.618	.168	-12.783	-.624	.157	-3.986
-12.0	-.575	.137	-10.870	-.579	.126	-4.581
-10.0	-.499	.109	-9.020	-.503	.101	-4.959
-8.0	-.416	.081	-7.183	-.419	.075	-5.565
-6.0	-.318	.056	-5.377	-.320	.053	-6.064
-4.0	-.144	.033	-3.717	-.145	.032	-4.521
-2.0	-.062	.022	-1.879	-.062	.022	-2.861
.0	.017	.018	-.033	.017	.018	.941
2.0	.097	.019	1.811	.097	.019	5.197
4.0	.176	.024	3.655	.177	.023	7.717
6.0	.261	.037	5.488	.263	.035	7.603
8.0	.335	.053	7.343	.337	.050	6.797
10.0	.405	.073	9.205	.407	.068	5.985
12.0	.476	.095	11.064	.480	.088	5.427
14.0	.542	.122	12.932	.547	.113	4.858
16.0	.605	.154	14.809	.611	.143	4.270
18.0	.664	.191	16.692	.671	.178	3.769
20.0	.732	.245	18.555	.741	.229	3.234
22.0	.796	.303	20.427	.806	.285	2.831
24.0	.854	.368	22.311	.866	.348	2.491
26.0	.914	.434	24.192	.927	.411	2.254
28.0	.964	.512	26.091	.979	.487	2.011
30.0	.997	.584	28.023	1.014	.558	1.816
32.0	1.025	.666	29.967	1.042	.640	1.628
34.0	1.015	.714	31.986	1.033	.690	1.497
36.0	.981	.759	34.051	.999	.739	1.352

8-2) Vortex Plate: g/Cr=0.01 U_∞=30m/s

Uncorrected			Corrected			
α	CL	CD	α	CL	CD	L/D
-14.0	-.632	.173	-12.756	-.638	.160	-3.977
-12.0	-.595	.142	-10.831	-.599	.131	-4.577
-10.0	-.516	.111	-8.986	-.520	.103	-5.044
-8.0	-.406	.078	-7.204	-.408	.073	-5.585
-6.0	-.269	.050	-5.472	-.271	.047	-5.702
-4.0	-.150	.030	-3.706	-.151	.030	-5.069
-2.0	-.064	.020	-1.874	-.065	.020	-3.198
.0	.017	.016	-.034	.017	.016	1.080
2.0	.097	.017	1.810	.097	.017	5.790
4.0	.175	.023	3.657	.176	.022	7.879
6.0	.259	.036	5.493	.260	.034	7.591
8.0	.330	.053	7.353	.332	.050	6.693
10.0	.399	.073	9.217	.402	.068	5.884
12.0	.466	.097	11.083	.470	.090	5.214
14.0	.527	.125	12.963	.532	.116	4.573
16.0	.587	.157	14.843	.593	.147	4.035
18.0	.648	.198	16.723	.655	.185	3.532

9-1) Vortex Plate: g/Cr=0.02 U_∞=20m/s

Uncorrected			Corrected			
α	CL	CD	α	CL	CD	L/D
-16.0	-.635	.204	-14.750	-.641	.192	-3.337
-14.0	-.620	.174	-12.780	-.625	.163	-3.845
-12.0	-.579	.145	-10.862	-.584	.134	-4.342
-10.0	-.511	.110	-8.997	-.514	.102	-5.061
-8.0	-.427	.081	-7.162	-.430	.075	-5.695
-6.0	-.286	.051	-5.439	-.288	.048	-5.942
-4.0	-.156	.032	-3.695	-.156	.031	-4.973
-2.0	-.069	.022	-1.865	-.069	.022	-3.206
.0	.011	.018	-.022	.011	.018	.630
2.0	.094	.019	1.816	.094	.018	5.153
4.0	.176	.024	3.656	.177	.023	7.677
6.0	.241	.032	5.527	.243	.030	7.963
8.0	.321	.047	7.371	.323	.044	7.387
10.0	.389	.063	9.236	.392	.058	6.709
12.0	.464	.085	11.088	.468	.078	5.989
14.0	.529	.113	12.959	.534	.104	5.112
16.0	.594	.150	14.829	.600	.139	4.315
18.0	.670	.195	16.680	.677	.182	3.728
20.0	.746	.253	18.528	.755	.237	3.186
22.0	.805	.307	20.410	.815	.289	2.825
24.0	.877	.379	22.266	.889	.357	2.491
26.0	.932	.446	24.156	.946	.422	2.240
28.0	.986	.521	26.047	1.001	.495	2.021
30.0	1.034	.600	27.951	1.050	.572	1.835
32.0	1.066	.683	29.886	1.084	.654	1.657
34.0	1.041	.726	31.934	1.060	.701	1.512
36.0	1.003	.766	34.007	1.022	.744	1.373

9-2) Vortex Plate: g/Cr=0.02 U_∞=30m/s

Uncorrected			Corrected			
α	CL	CD	α	CL	CD	L/D
-16.0	-.650	.212	-14.719	-.657	.199	-3.298
-14.0	-.641	.181	-12.739	-.647	.168	-3.849
-12.0	-.600	.148	-10.821	-.605	.137	-4.423
-10.0	-.509	.111	-9.001	-.512	.103	-4.956
-8.0	-.416	.082	-7.184	-.418	.076	-5.490
-6.0	-.252	.048	-5.505	-.254	.046	-5.458
-4.0	-.161	.032	-3.685	-.161	.031	-5.198
-2.0	-.072	.020	-1.859	-.073	.020	-3.576
.0	.011	.016	-.022	.011	.016	.702
2.0	.095	.017	1.814	.096	.017	5.649
4.0	.175	.023	3.657	.176	.022	7.891
6.0	.241	.032	5.528	.242	.030	7.991
8.0	.315	.046	7.382	.317	.043	7.341
10.0	.384	.063	9.246	.386	.059	6.576
12.0	.453	.086	11.109	.457	.080	5.743
14.0	.516	.115	12.985	.520	.107	4.857
16.0	.581	.155	14.855	.587	.145	4.054

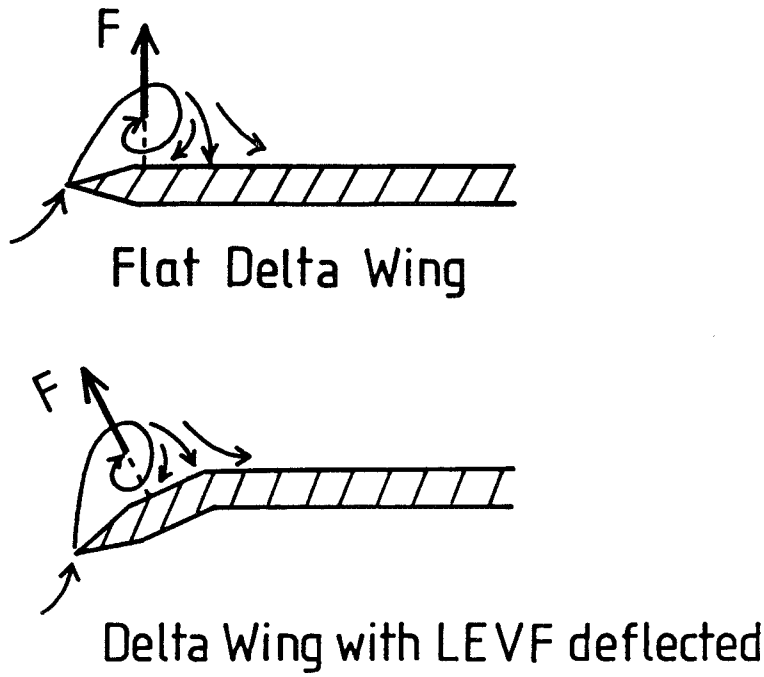

a) Vortex Flap

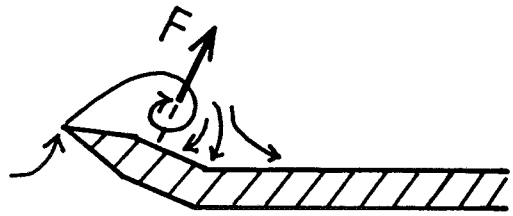

b) Inverted Vortex Flap

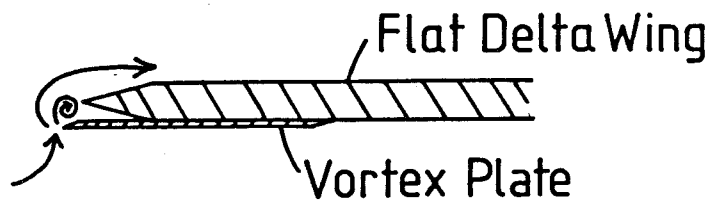

c) Vortex Plate

Fig.1 Concept of Vortex Flap and Vortex Plate

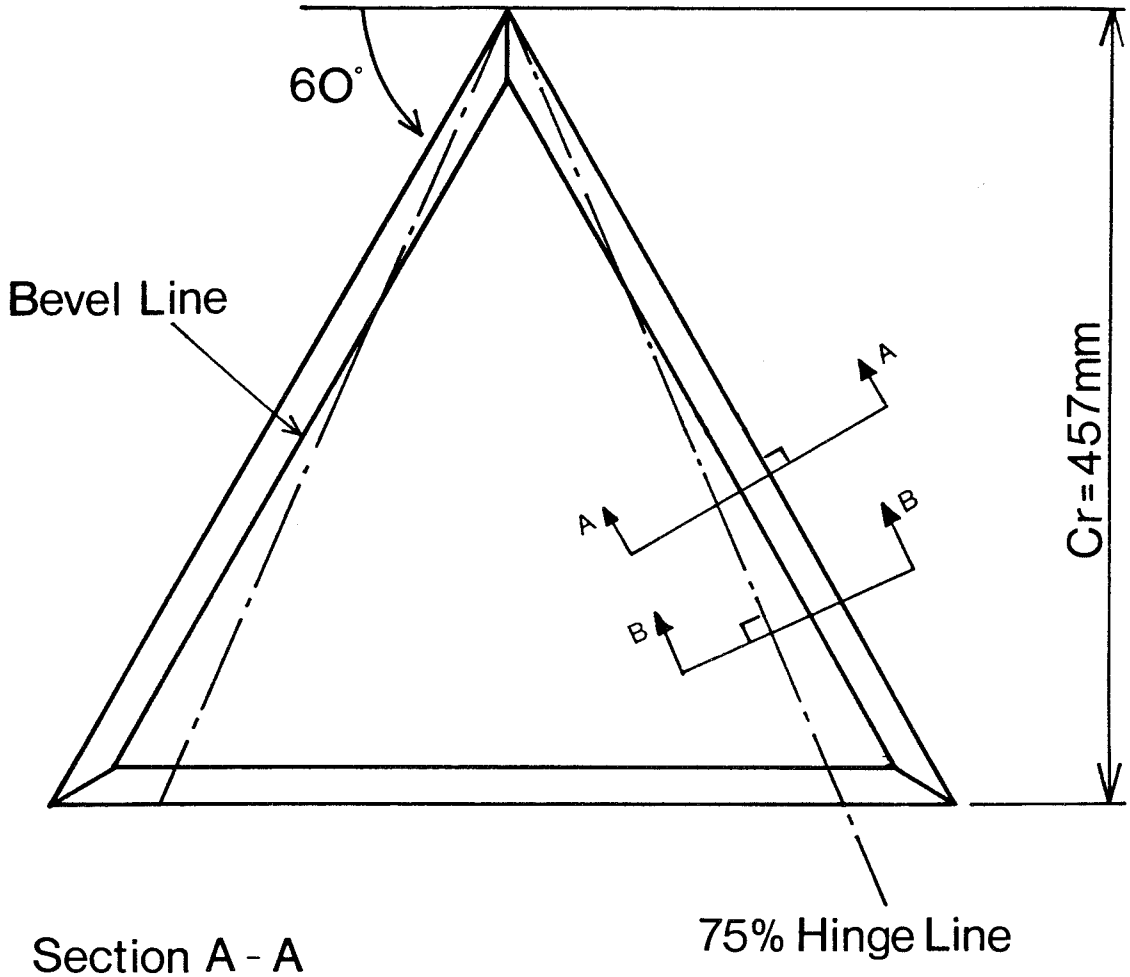

Section A - A

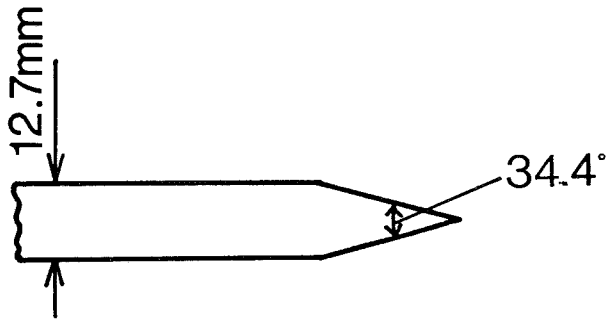

Section B - B with LEVF deflected

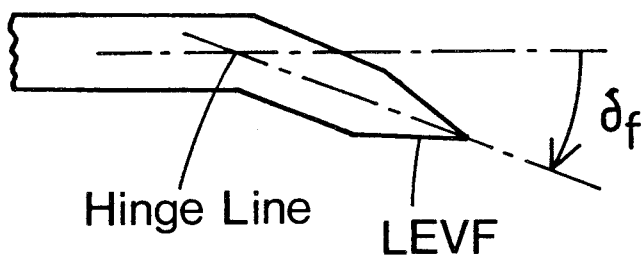

Fig.2 Delta Wing Model with LEVF

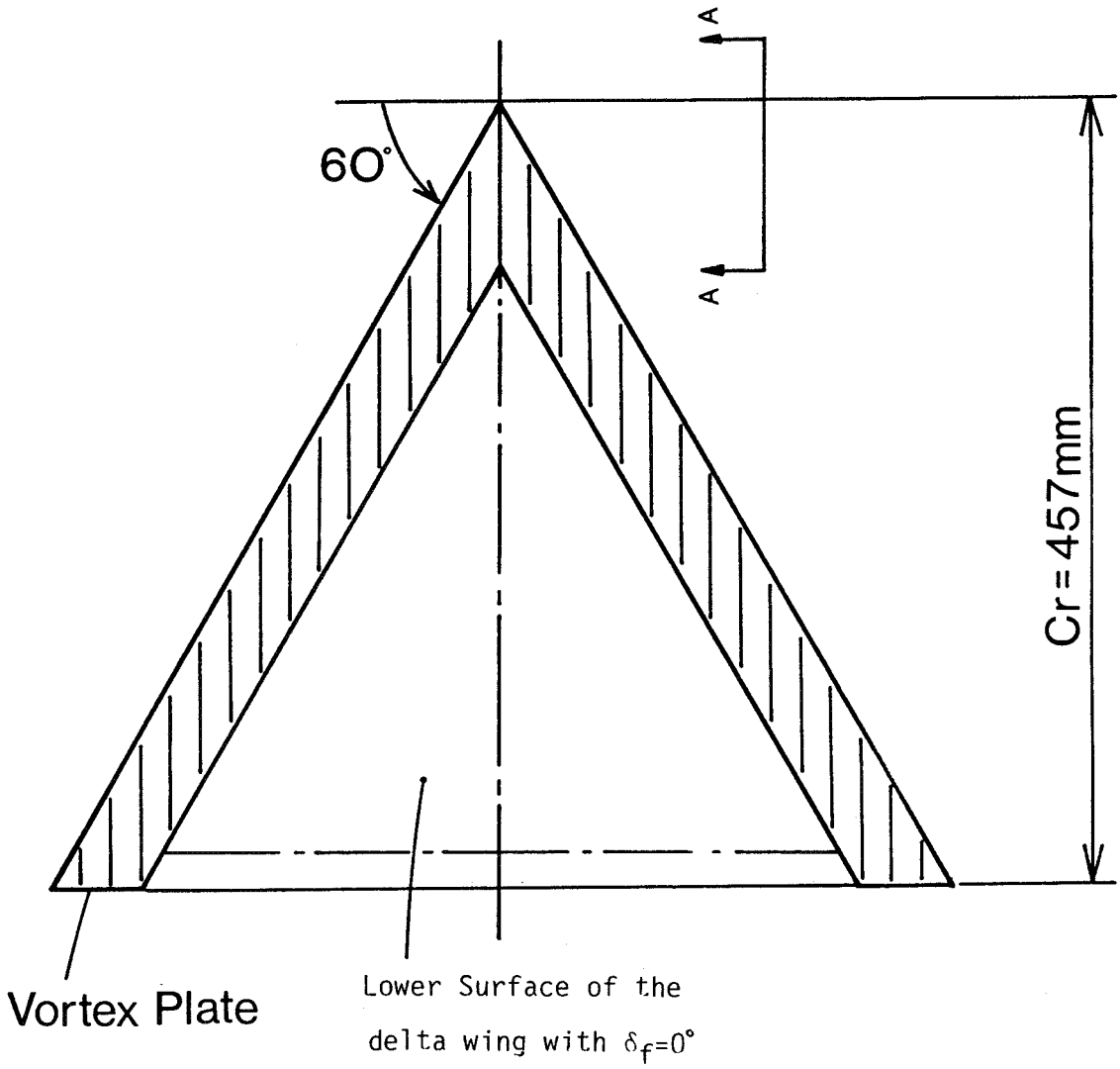

Chordwise section A-A through L.E.

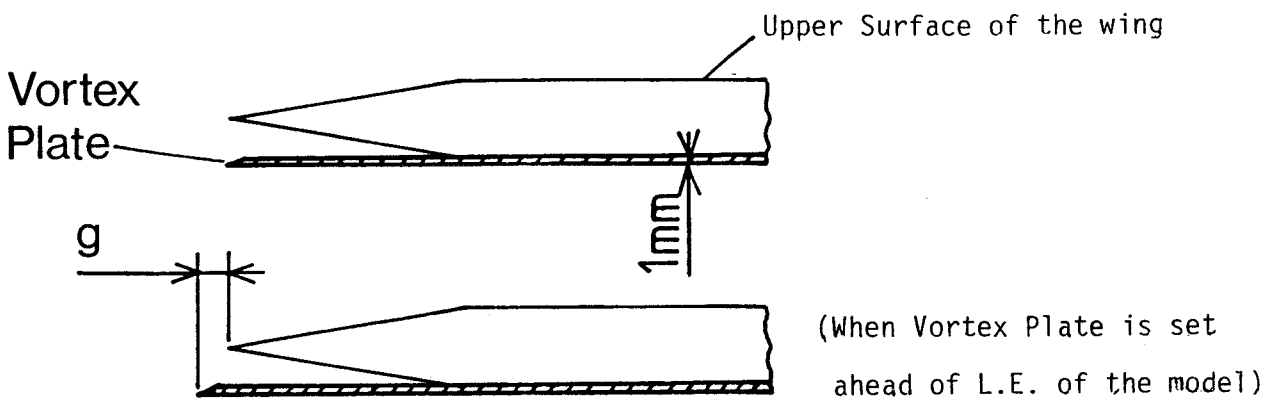

Fig.3 Delta Wing Model with Vortex Plate

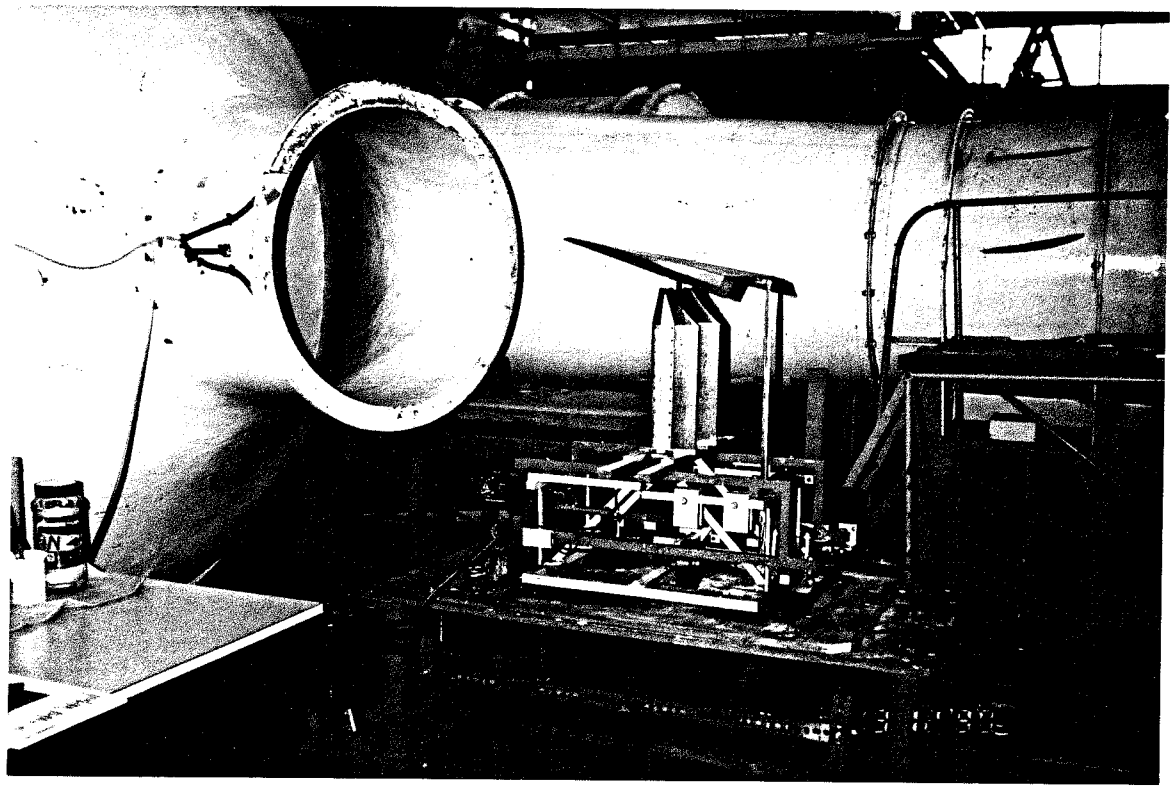

Fig.4 Wind Tunnel, Model Mounting and Tunnel Balance

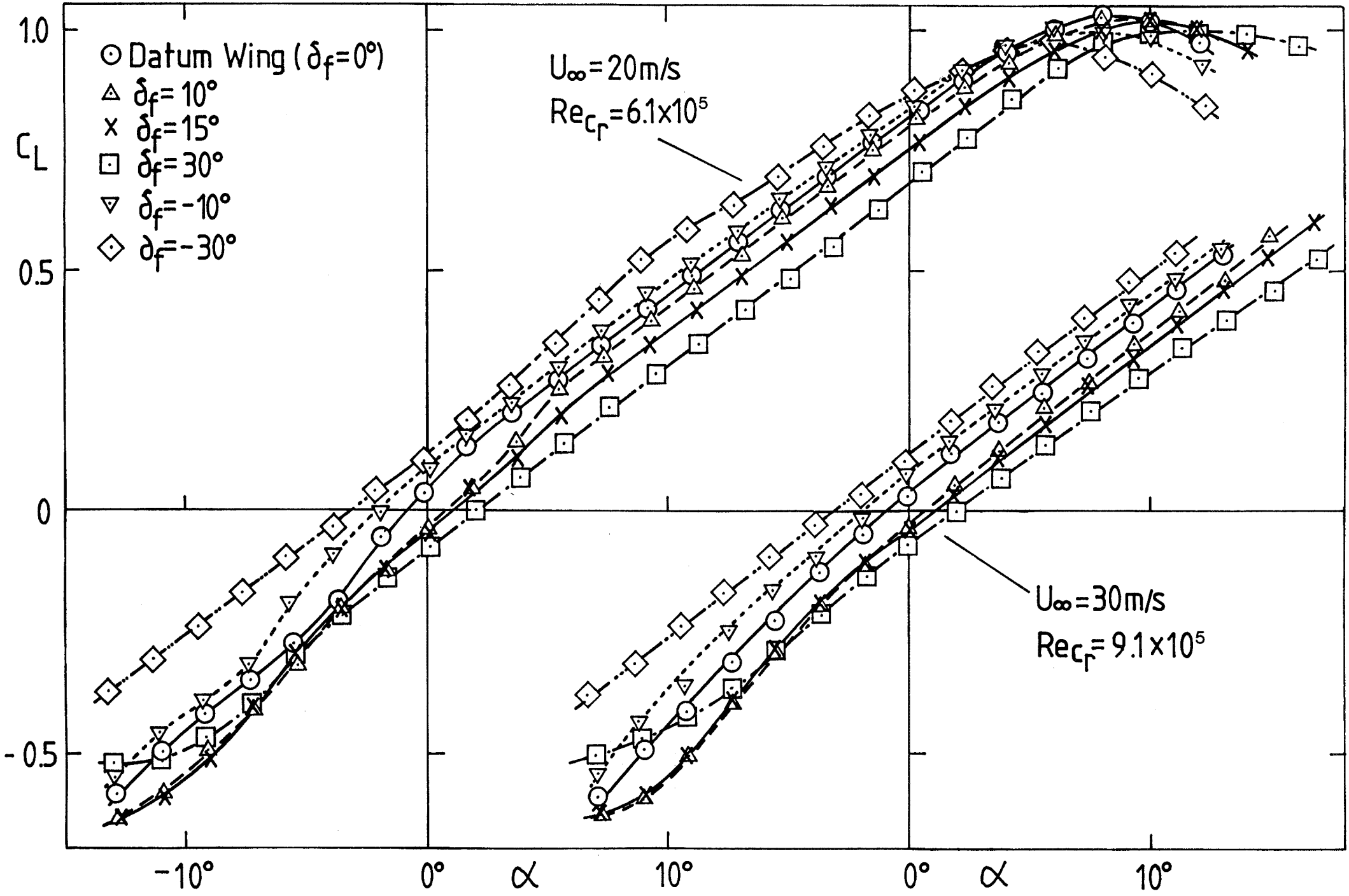

Fig.5 Effect of LEVF on C_L vs. α

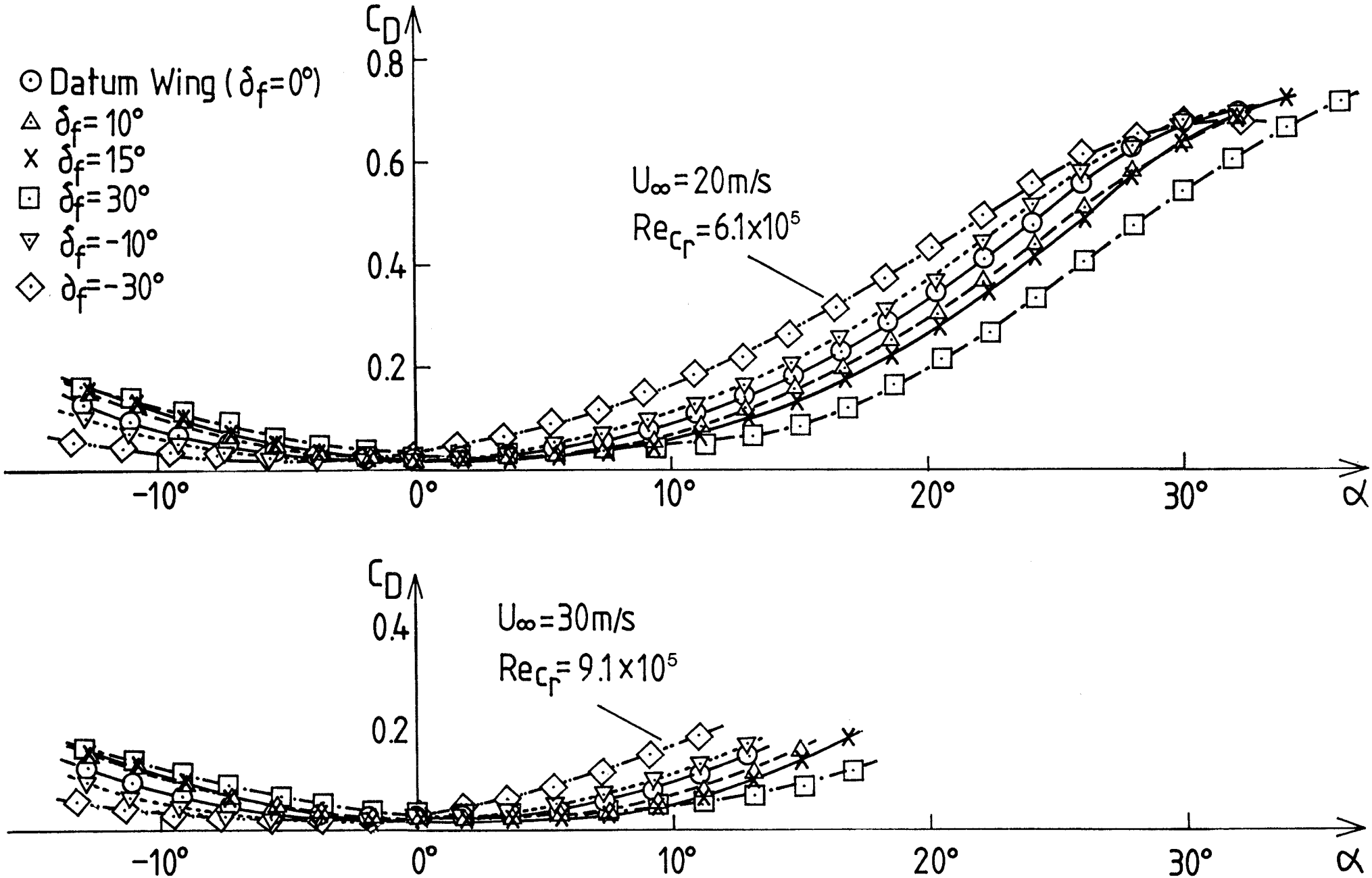

Fig.6 Effect of LEVF on C_D vs. α

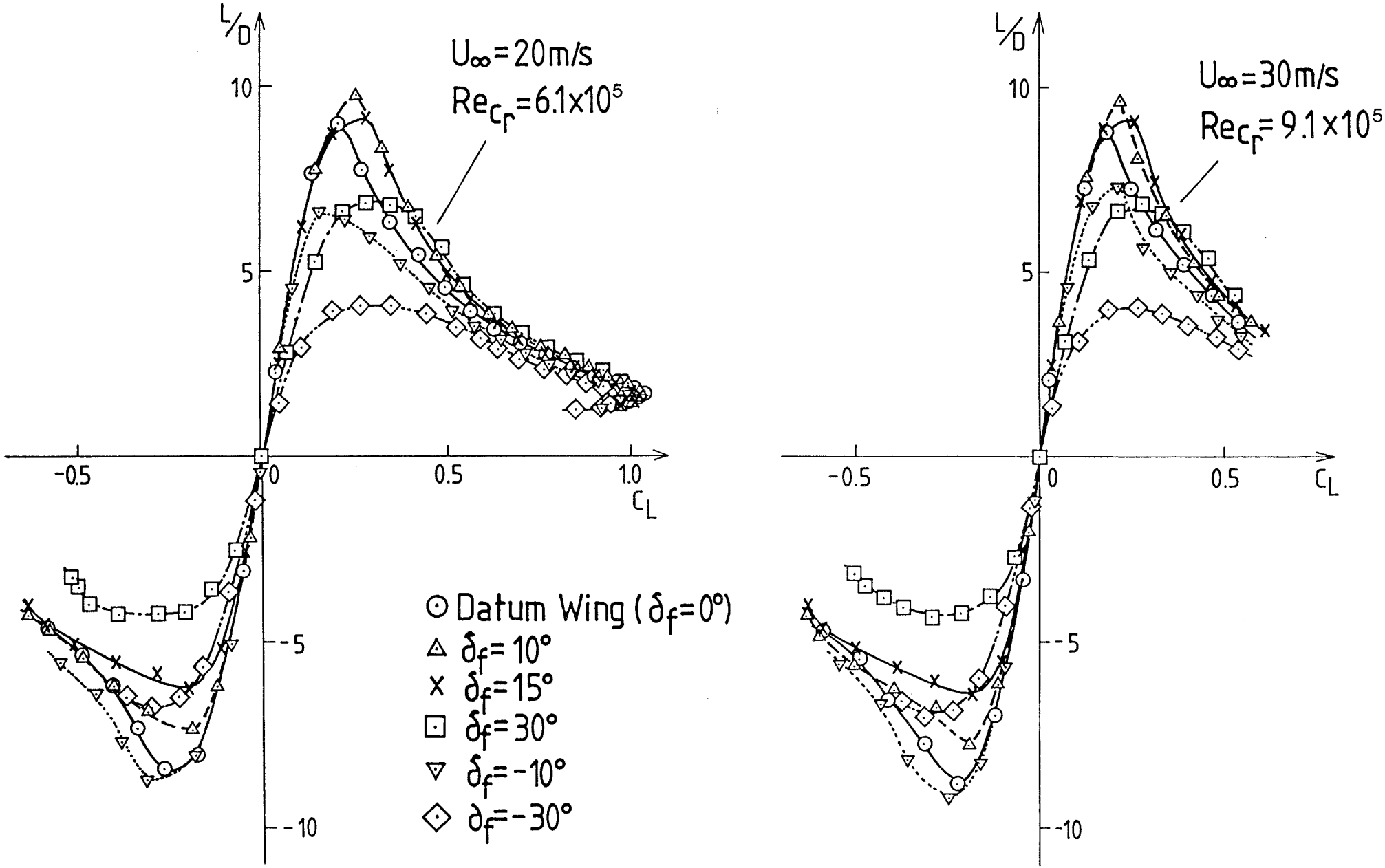

Fig.7 Effect of LEVF on L/D vs. C_L

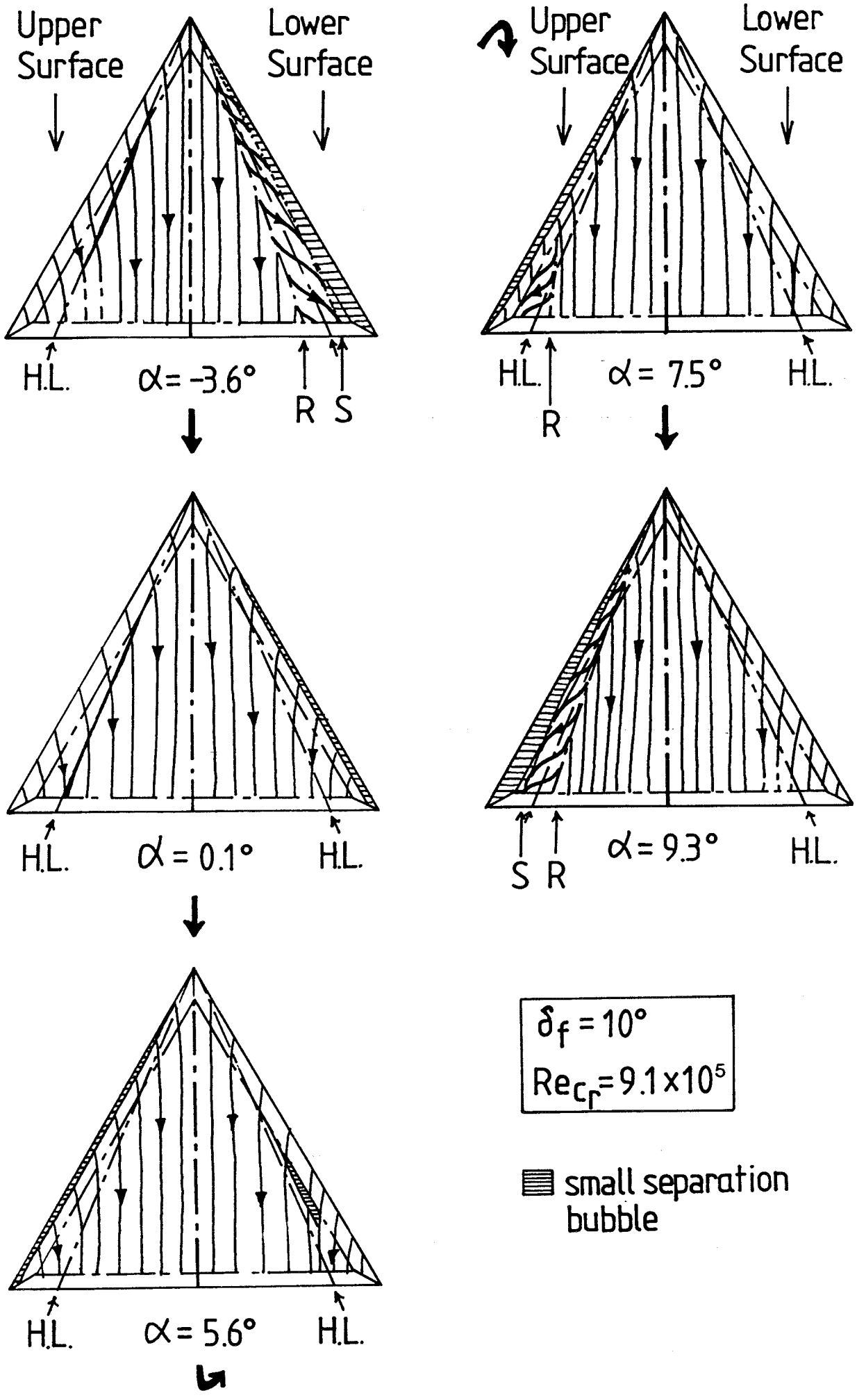

Fig.8 Surface Flow Patterns (δ_f=10deg)

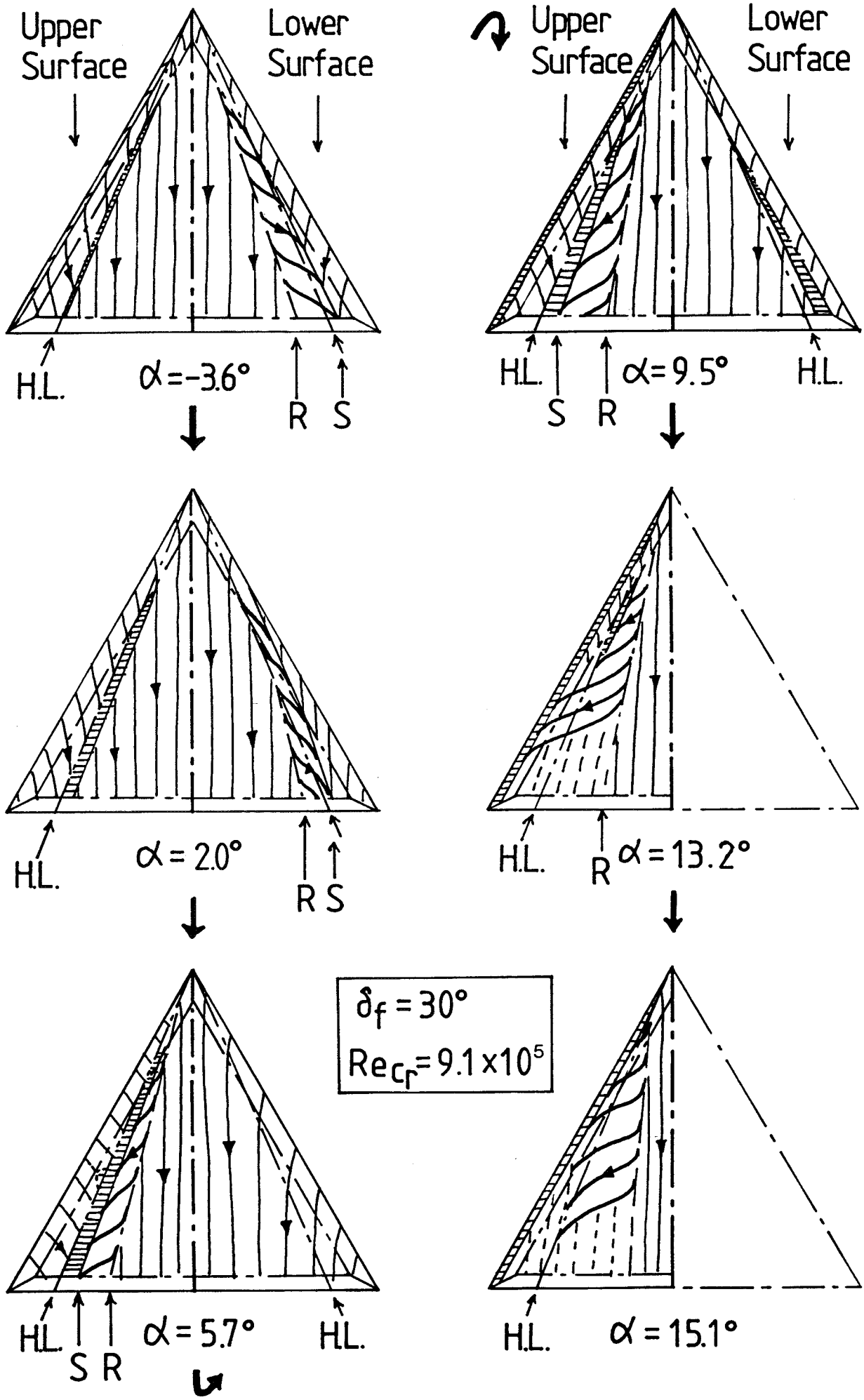

Fig.9 Surface Flow Patterns (δ_f=30deg)

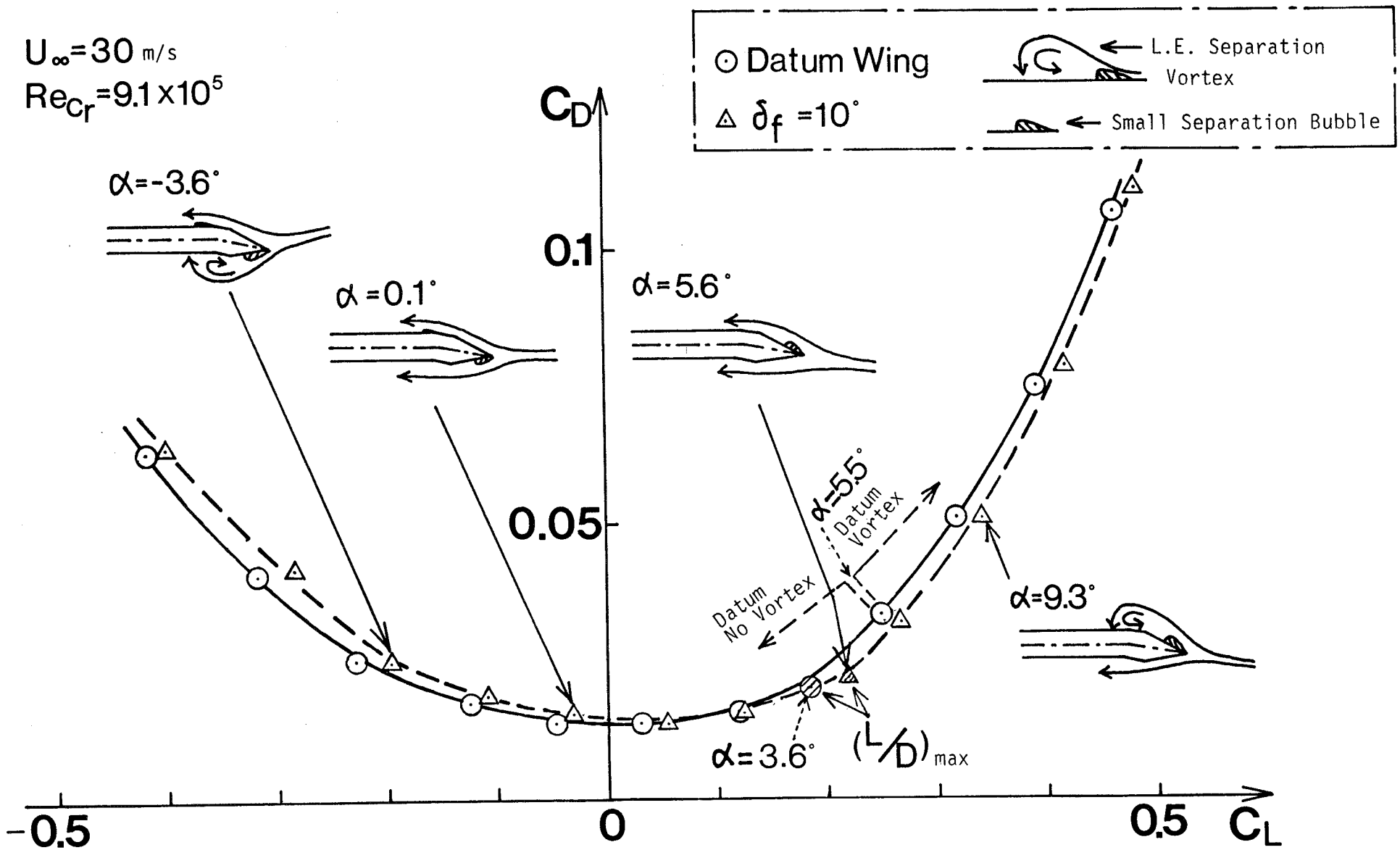

Fig.10 C_D vs. C_L and Cross Flow Patterns (δ_f=10deg)

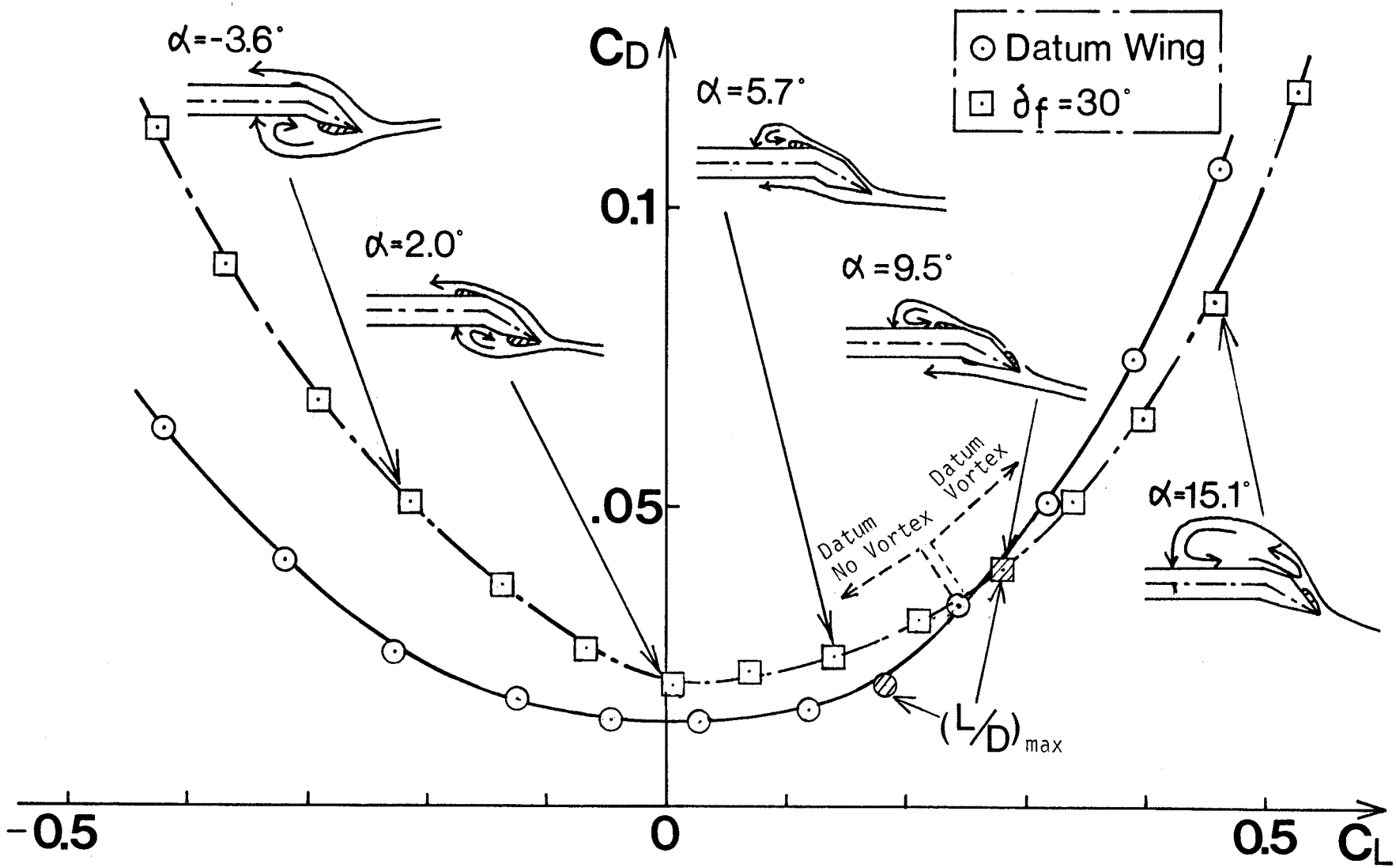

Fig.11 C_D vs. C_L and Cross Flow Patterns (δ_f=30deg)

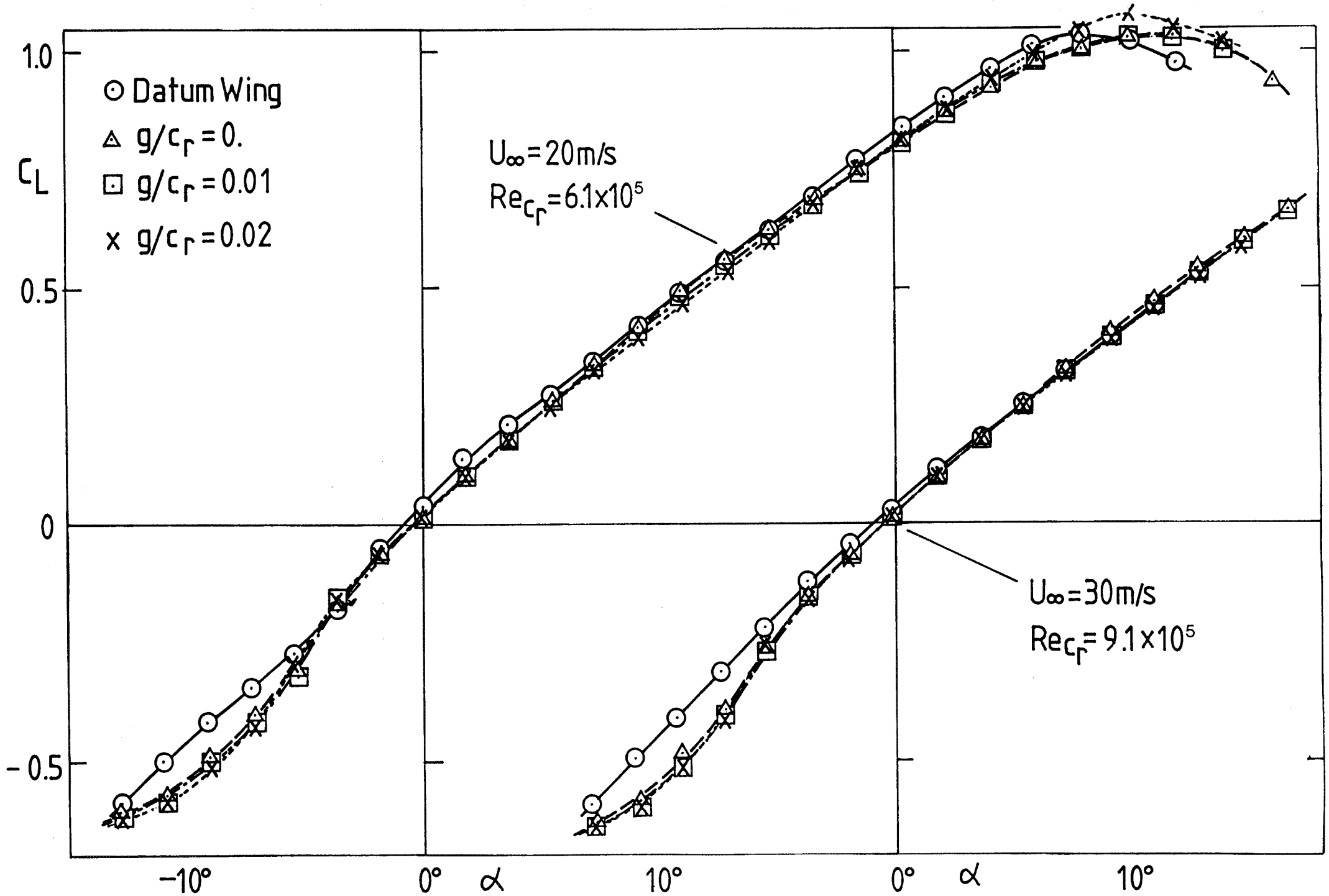

Fig.12 Effect of Vortex Plate on C_L vs. α

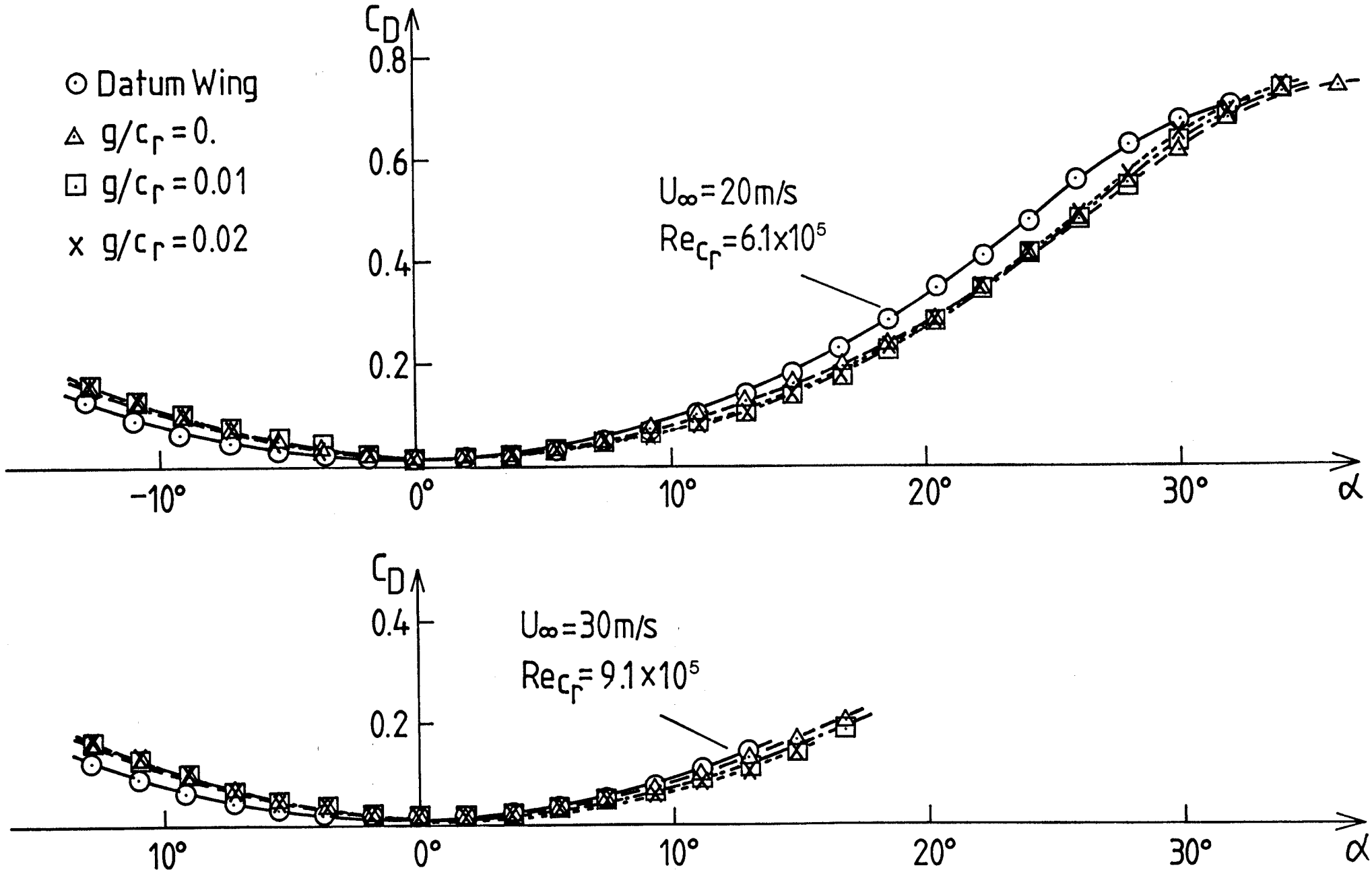

Fig.13 Effect of Vortex Plate on C_D vs. α

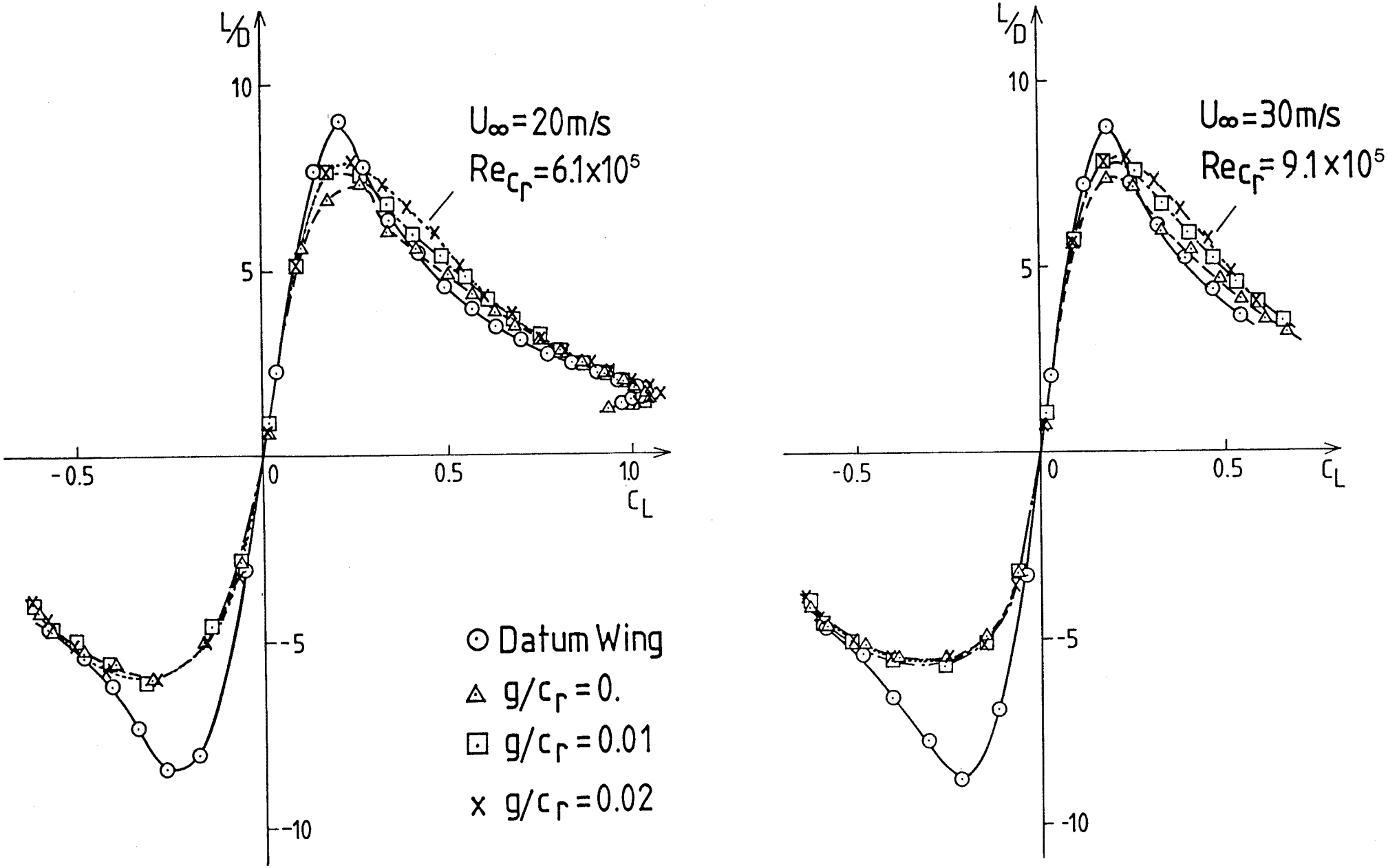

Fig.14 Effect of Vortex Plate on L/D vs. C_L

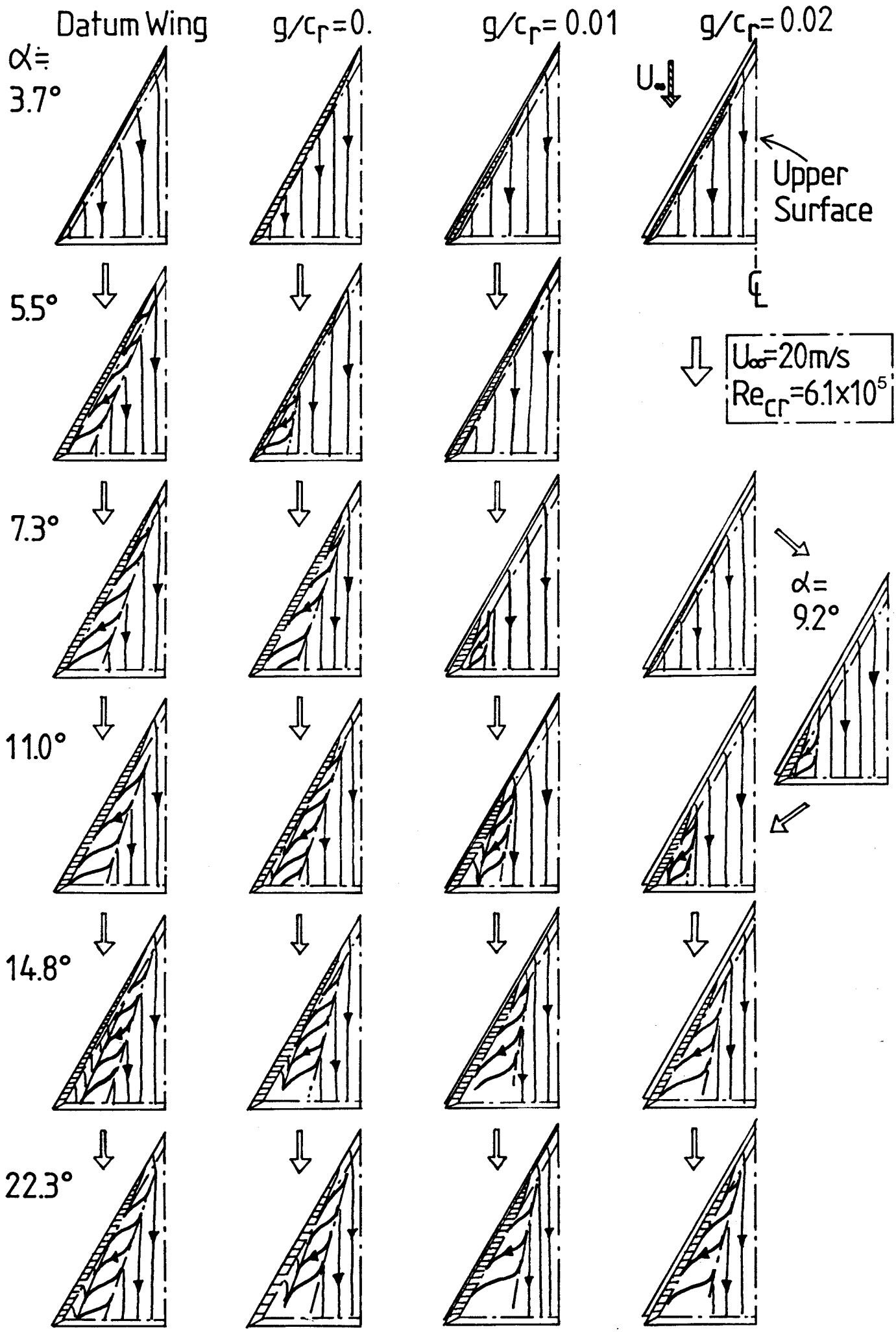

Fig. 15 Surface Flow Patterns with and without Vortex Plate

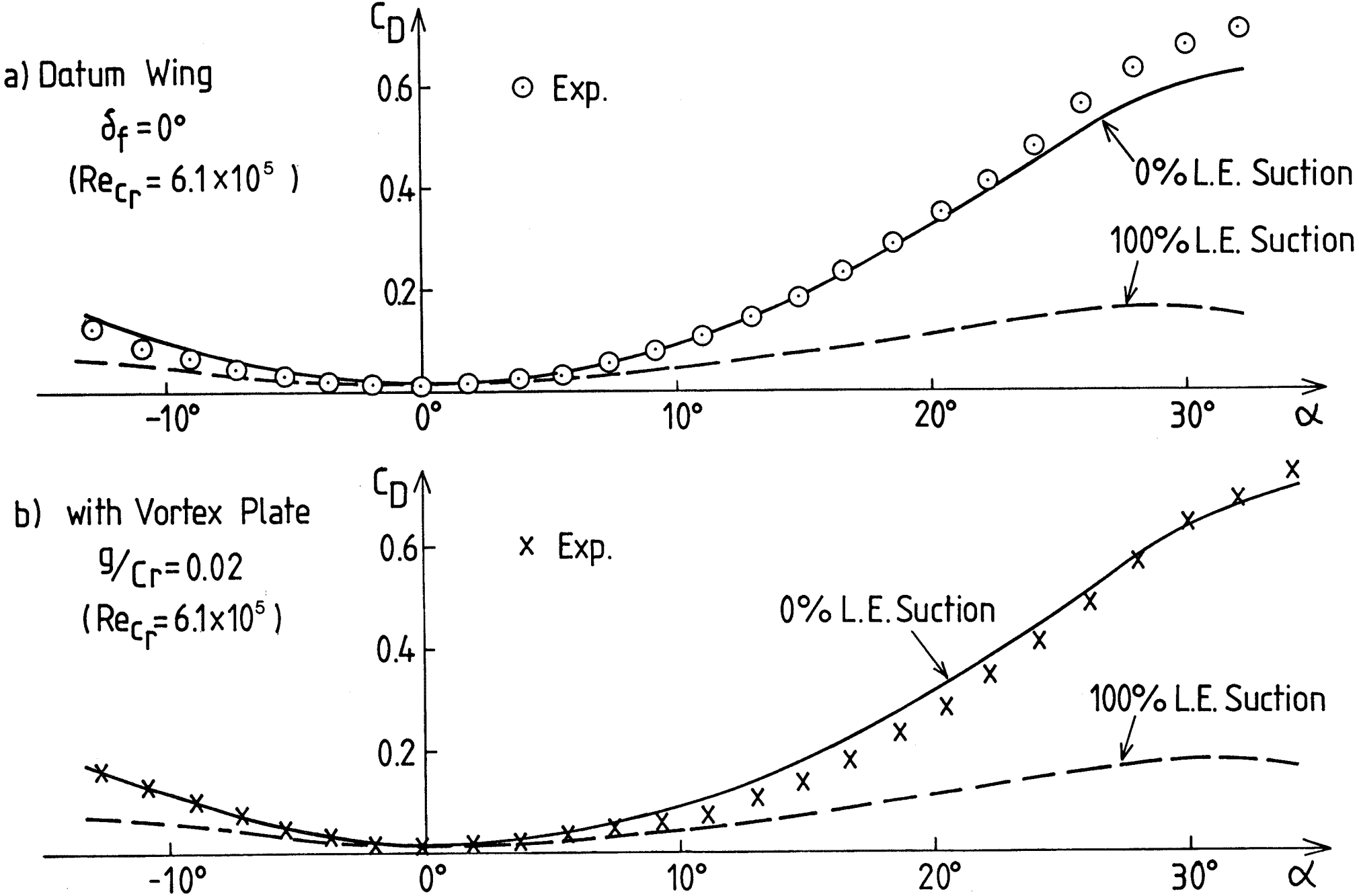

Fig.16 Effect of Leading-Edge Suction Force on C_D (Datum Wing & g/Cr=0.02)